Design of a low-grade heat to power conversion system, using flow batteries

By

Jorrit Bleeker

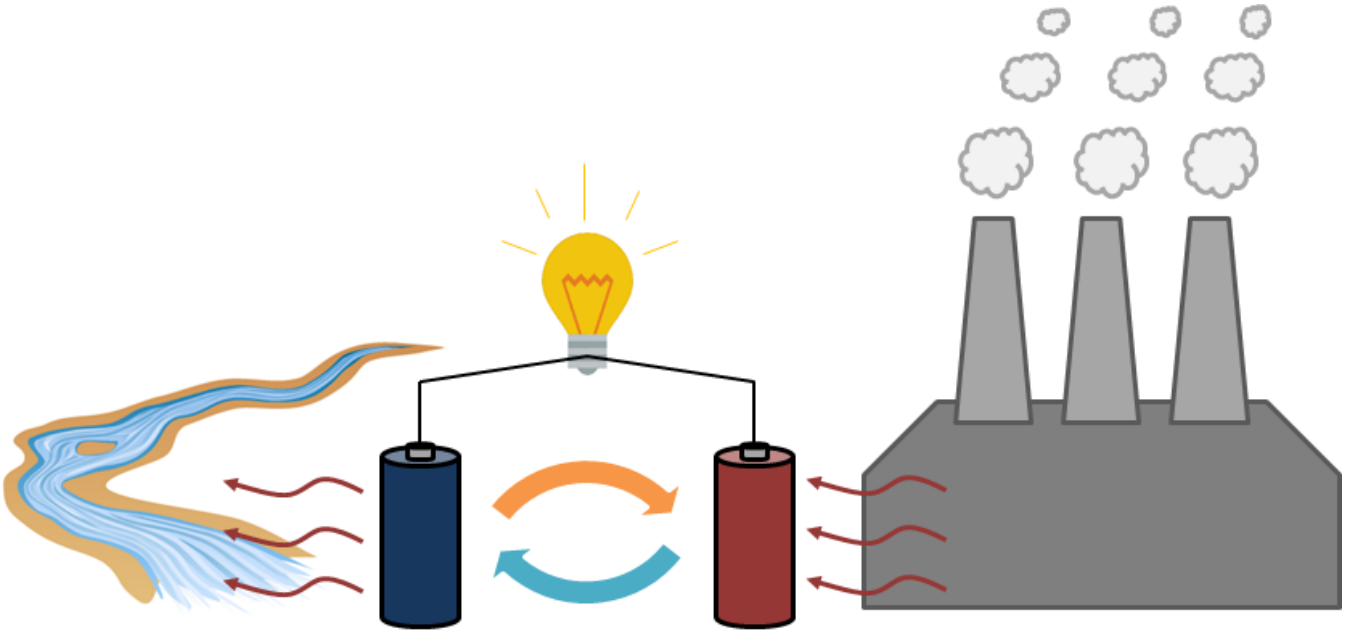

in partial fulfilment of the requirements for the degree of

Master of Science
in Chemical Engineering

at the Delft University of Technology,
to be defended publicly on Wednesday July 5th, 2017 at 10:00

Supervisor:	Dr. David A. Vermaas
Thesis committee:	Prof. dr. Fokko M. Mulder
	Dr. Volkert van Steijn

TU Delft

Abstract

For every Joule of electricity produced in power plants today, around two Joules are thrown away. The majority of this wasted energy is in the form of low grade (<100 °C) waste heat. Currently no technology exist that can effectively convert this heat back into a useful form of energy, such as electricity.

The goal of this thesis is to take a new approach to heat to power conversion, using the thermally regenerative electrochemical cycle (TREC) with flow batteries. The TREC makes use of the Seebeck effect, which is the change of (redox) potential due to a change in temperature. The potential difference between a cold and hot battery can then be used to generate electricity. The driving parameter is this system is the Seebeck coefficient, which gives the potential change per unit temperature (mV/K).

The TREC system was designed in three steps. (i) A flow battery consists of two electrolytes, for the TREC these electrolytes need to have large and opposite Seebeck coefficients. A large screening and characterization of the electrolytes was done to finally select two for the TREC. (ii) The parts of the flow cell were custom designed and built. The performance of the flow cell was tested with the two selected electrolytes. (iii) Using experimental parameters from the previous step, a model was created with ASPEN Plus to determine the efficiency and power output from a TREC system.

Acknowledgements

First of all I would like to thank David for supervising me throughout the project and giving me the possibility (and responsibility) to do this amazing project. And also for being supportive while I spent the whole thesis working part time as a teaching assistant, doing an Honours project and preparing high school students for their exams.

I am very grateful to Damla Inan and Ferdinand Grozema for giving me the opportunity to start a master thesis project in the OM group. I decided to quit the project after only one and a half week. They accepted this decision and still treat me as a friend every time we meet.

Thanks to the two committee members, Volkert van Steijn and Fokko Mulder who made time in their agendas to allow me to defend. And to Remco Hartkamp who offered to join the committee but sadly cannot make it due to a conference, but gave some interesting meetings on the simulation of electrolytes to find the Seebeck coefficient.

I would not have been able to create the flow cell if it was not for Stefan and Reinier from DEMO who taught me how to use Autodesk Inventor and gave me tips on the design and what materials to use. I also would like to thank Marcel that helped me with every little request I had at the workshop, even he was not even supposed to help me. Without Chirstiaan my whole lab experience would have been a disaster, always jumping in when my clumsy hands could not complete the job, and being a great guy to work with in general. Thanks to Rajeev Dubey and Wolter Jager for helping me with suggestions on the synthesis of ACA, and for doing the NMR measurements for me. I am also very glad that Damla borrowed me her cuvettes for the UV-VIS spectrometry, and that Ruben Abellon supervised me while doing the measurements.

In the last two weeks two bachelor students joined me in my research for their LO1 course. Thanks, Barry and Lianne, for doing a lot of CV-measurements!

My time in the lab would not have been the same if it was not for the great company of Johan, Tets, Tessa and Aswin. And the company of Amit and Vera really helped in the late nights of writing the thesis. Thanks as well to Joep, Kača, Koen, Maulik and my mother for all reading a chapter of the thesis to check for spelling mistakes.

Finally, I would not have been able to finish the thesis without the support of my friends and family, in particular the following people helped to get to the end ☺: Máté, Ági, Kača, Romana, Koen, Joep, Eva, Fran, Sneha, Anirudh and Maxime. And of course the TP group for letting me be a part of their team.

Table of contents

List of abbreviations

Abbreviation	Description
ACA	Alloxazine carboxylic acid
ACA-2H	Reduced form of Alloxazine carboxylic acid
CuHCF	Copper hexacyanoferrate
CV	Cyclic voltammetry
DMSO	Dimethylsulfoxide
$Fe(CN)_6$	Hexacyanoferrate
ORC	Organic Rankine cycle
RFB	Redox flow battery
TREC	Thermal reversible electrochemical cycle
SHE	Standard hydrogen electrode (reaction)
V-RFB	All-vanadium redox flow battery

List of symbols

Symbol	Description	Units
C_P	Heat capacity (at constant pressure)	J/(mol*K)
d	Channel thickness	m
E	Potential	V
E_0	Potential at reference temperature	V
$E_{1/2}$	Half-cell potential	V
E_{loss}	Potential losses	V
E_{OC}	Open Cell potential	V
E_{pa}	Anodic peak potential	V
E_{pc}	Cathodic peak potential	V
F	Faraday's constant	96485 C/mol
ΔG	Gibbs free energy change	J/mol
ΔH	Enthalpy change	J/mol
I_{dens}	Current density	A/m^2
It	State of charge	C
L	Channel length	m
n	Stoichiometric constant of electrons in redox reaction	-
P	Power	W
p	Pressure	Pa
P_{max}	Maximum power density	W/m^2
Q_{charge}	Charge put in during charging	C
$Q_{discharge}$	Charge gained back during discharging	C
Q_{HX}	Energy required to heat after heat exchanger	J
Q_{loss}	Energy losses	J
R	Ohmic resistance (times unit area)	Ωm^2
R	Ideal Gas constant	8.314 J/(mol*K)
R_0	Ohmic resistance at reference temperature	Ωm^2
R_{int}	Internal resistance (times unit area)	Ωm^2
ΔS	Entropy change	J/(mol*K)
S*	Eastman entropy	J/(mol*K)
$\bar{\bar{S}}_e$	Total transported entropy of the electrons in the electrode	J/(mol*K)
T	Temperature	ºC or K
T_0	Reference temperature	ºC or K
T_{cold}	Temperature of the heat sink	ºC or K
T_{hot}	Temperature of the heat source	ºC or K
V	Voltage	V
w	Channel width	m
α	Seebeck coefficient	V/K
α_{full}	Full cell Seebeck coefficient	V/K
η	Heat to power efficiency	-
η_C	Current efficiency	-
η_{Carnot}	Carnot efficiency	-
η_{pump}	Pump efficiency	-
θ	Temperature coefficient	$ºC^{-1}$
μ	Dynamic viscosity	Pa·s

List of figures

1. Introduction

For every Joule of electricity produced in power plants today, around two Joules of energy are wasted[1, 2]. This wasted energy is predominantly in the form of thermal energy. Especially in an age where fossil fuels are running out, and carbon emissions have to be minimized, it is vital to utilize this wasted energy stream. Various techniques already exist to employ waste heat, for example as heat source for other nearby plants and greenhouses or the heating of houses in neighboring rural areas[3]. Waste heat can also be converted into electricity by creating steam for steam turbines, which can even be used for smaller applications, like charging a car battery from the heat of the engine[4].

The major part of waste heat, however, consists of so-called low-grade waste heat (~100°C and lower) which is usually not of sufficient high temperature for the applications mentioned above[5]. Therefore it is required to use other technologies to convert this low-grade waste heat into a more useful form of energy (e.g. chemical bonds or electricity). At the moment there is no mature technology that is widely used to recover low-grade waste heat. A reason is the difficulty that comes with converting low-grade heat into work, since you work against the 2nd Law of thermodynamics. The maximum efficiency (heat converted into work) a heat engine can obtain was already described in 1824 by Sadi Carnot[6], and hence is called the Carnot efficiency:

$$\eta_{Carnot} = 1 - \frac{T_{cold}}{T_{hot}} \qquad \textbf{(1)}$$

Here T_{cold} and T_{hot} represent the temperature (in K) of a heat sink (e.g. river water) and a (low-grade) heat source respectively. Since the temperature difference between low-grade heat and atmospheric temperatures is small, only low efficiencies (see Table 1) can be obtained. So in a perfect scenario at most only 21 % of low grade heat (100 ºC) can be converted into work!

Heat energy is predominantly converted into power using steam turbines. Steam turbines cannot be used for low grade waste heat, since water has a boiling point of 100 °C. In the Organic Rankine Cycle (ORC) (Figure 1A) a similar turbine is used, with an organic solvent instead of water as working fluid. The ORC has proven to be a solution with heat to power efficiencies up to 7%[7] (cycled between 25-116 °C), which is 30 % of the Carnot efficiency.

Table 1. Calculated Carnot efficiencies for various values of T_{cold} and T_{hot} using **(1)**, which are the temperatures of the heat sink (in this case the temperature of river water in the Netherlands in May[8]) and low-grade waste heat source.

T_{cold}/T_{hot} (°C)	η_{Carnot}
20/100	21.44%
20/80	16.99%
20/60	12.01%
20/40	6.39%

A completely different approach is by converting heat into electricity through the thermoelectric effect, or **Seebeck effect** (see next page). Thermoelectric generators (Figure 1B) are one of the technologies that use this approach. The efficiency of these generators is low compared to the ORC (maximum of 3% for the temperature interval 25-80 °C)[9]. Thermoelectric generators do not require moving parts or organic solvents at elevated pressures and temperatures. These generators are therefore much safer to use, in addition to having a lower operating cost. However, state-of-art thermoelectric generators require a high capital investment, since they mostly consist of rare materials such as Tellurium and Selenium[9].

Seebeck effect
The Seebeck effect is a thermo-electric effect. A (semi)conducting material will create a voltage when two sides of the material are held at a different temperature[10]. The same happens for redox active compounds, of which the redox potential changes with temperature. The voltage difference is defined as follows: $\boldsymbol{\Delta V = \alpha \Delta T}$
Here α is the so called Seebeck coefficient of the material, and has units of V/K:

- For metals, this is in the order of 1 μV/K
- For semiconductors, 300-500 μV/K
- For redox reactions, 0.5-2 mV/K.

The Seebeck coefficient can be positive or negative.

Very close to thermoelectric generators are thermogalvanic cells (Figure 1C). In a thermogalvanic cell, the temperature dependence of the redox potential is exploited to convert heat into electricity. Usually only one soluble redox couple is used, of which the oxidation and reduction reaction each happen at one of the electrodes. However thermogalvanic cells suffer from efficiency losses, due to diffusion required between the electrodes and a thermal gradient that has to be maintained[11]. According to a review by Gunawan *et al.*, the highest heat to power efficiencies only reached 2.6% of the Carnot efficiency[12].

Recently in 2014, scientists from MIT published[13] a new type of heat recovery system that makes use of the Seebeck effect, which authors named a Thermal Regenerative Electrochemical Cycle (TREC). The TREC uses a Cu/Cu^{2+} and Copperhexacyanoferrate battery, of which the (dis)charge potential is strongly dependent on the temperature. To harvest thermal energy, the entire device undergoes a cycle consisting of 4 steps: Heating up, Charging, Cooling down and discharging (see Figure 1D)[13]. Less energy will be used for charging, than is gained back by discharging, so there is net energy gain. Without any heat recuperation, the system already reaches almost 25% of the Carnot efficiency (3.7% heat to power), when cycled between 10 and 60 °C. If there would be 100% heat exchange efficiency, it even goes up to 80% (12% heat to power).

A big downside of this system is that it consists of solid materials. The battery needs to be fully charged, and then moved to a cool place to be cooled down. Once cool, it will be fully discharged and then moved to a heat source again to go to a higher temperature again. The heat transfer itself is also not straightforward. One needs to press the battery against the heat source or sink with thermal paste on both objects to allow the heat transfer[13]. For heat recovery, hot and cold batteries need to be pressed together. These steps are time consuming and significantly reduce the power output of the system.

In this thesis, a new approach to the TREC will be investigated. Instead of regular solid batteries, a system based on redox flow batteries (RFB) will be designed. A RFB is a battery that does not use solid electrodes, but of soluble redox couples in water (RFBs will be explained in more detail in Chapter 2). Since the active compound in a RFB is dissolved in a liquid, it can easily be pumped from a hot to a cold place and through a heat exchanger, which solves both problems of the TREC described above. The goal of this thesis is to design and build such a setup, inspired by flow batteries, to convert low grade waste heat into electricity and to see how efficient can be.

The report will be structured in the following manner: First the background theory will be explained and some literature will be reviewed in chapter 2. At the end of chapter 2 the research questions and goals will be formulated. Chapter 3 shall discuss the experimental setups and conditions. Then in chapter 4 the experimental results will be shown and discussed. After that the conclusions will be presented, followed by recommendations for future studies. There are seven Appendices at the end of the report.

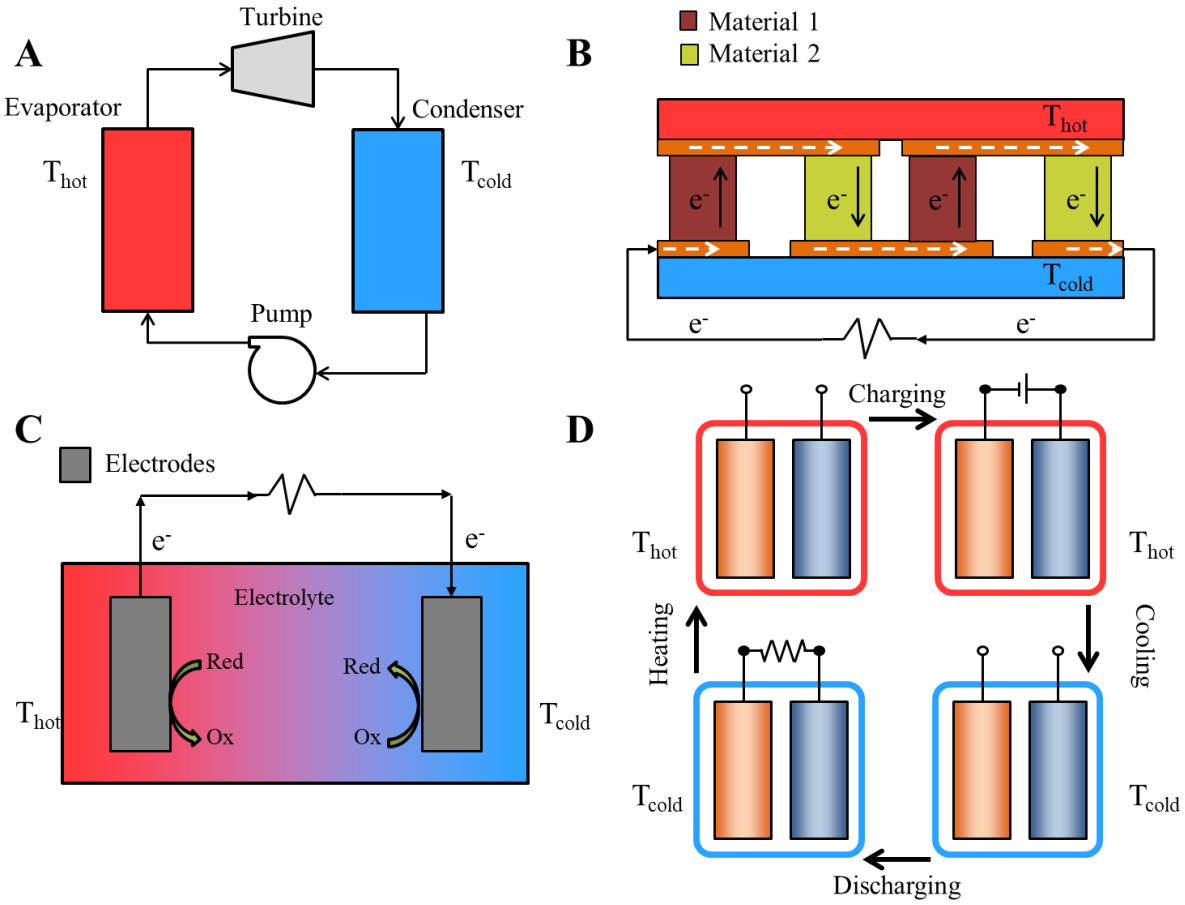

Figure 1. Schematic diagrams of various technologies that are used for low grade waste heat recovery. In every diagram the hot and cold sides are marked by T_{hot} and T_{cold} respectively. **A**. Organic Rankine Cycle (ORC). A working fluid with boiling point lower than water is pumped through an evaporator, passed through a turbine, where the expansion of the vapor is converted into electricity. Then the vapor condenses in the condenser, and the cycle starts over again[14]. **B.** Thermoelectric generator. By using making use of two materials with a different Seebeck coefficient, a temperature difference is converted into a voltage, which will be converted into electrical power. **C.** Thermogalvanic cell. In a thermogalvanic cell the temperature dependence of a redox reaction is converted into electricity. By having two electrodes at different temperatures a potential difference is created, which is used to generate electrical power. **D.** Thermally regenerative electrochemical cycle (TREC) (figure inspired by Lee et al [13]). Like in a thermogalvanic cell, thermal energy is harvested through the Seebeck effect of a redox reaction. A battery consisting of materials with high Seebeck coefficients is charged at a different temperature than it is discharged. During this cycle, more energy is gained during the discharge, than was consumed during the charging.

2. Background theory and methods

This chapter will cover the background theory that was used in this thesis. First the driving force of batteries, redox reactions, will be discussed. Secondly the working principles of a redox flow battery (RFB) will be explained. Then the thermodynamic background of the Seebeck coefficient will be treated. Using this, the TREC will be explained. After that two relevant examples from literature will be discussed in more detail. Next some requirements for the parts of the designed setup will be given. Finally the research goal and questions of this thesis will be formulated.

2.1. Redox reactions

The crux of a battery is the redox reaction happening in the half cells. A redox reaction is a chemical reaction in which electrons are transferred between two species:

$$A + ne^- \rightarrow B$$

For a half reaction like the one above, the electrochemical potential can be related to Gibbs energy with the Nernst-Lewis-Latimer convention:

$$\Delta G = -nFE \quad \textbf{(2)}$$

Here ΔG is the Gibbs energy change for the reaction, n is the amount of electrons that are exchanged, F is the Faraday constant (96485 C mol^{-1}) and E is the half-cell potential of the reaction. For dissolved materials, the half-cell potentials can be measured easily versus a reference potential by a technique called cyclic voltammetry (CV)[15]. (See Figure 2)

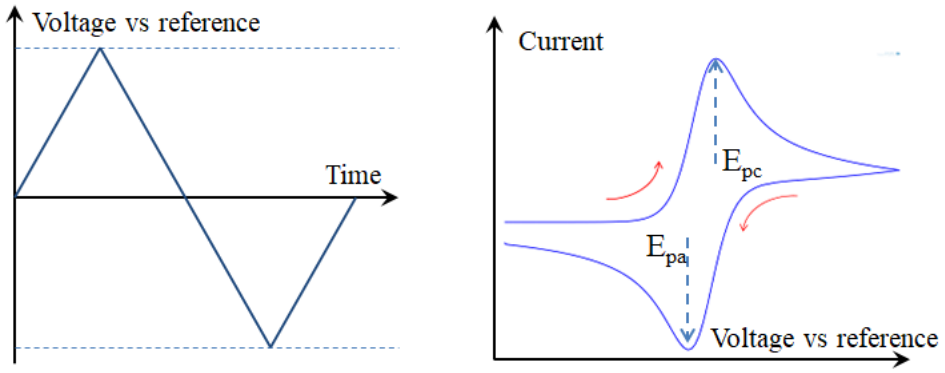

Figure 2. **Left:** The voltage (versus a reference reaction) is typically changes in a CV measurement, the slope is called scan rate. Usually multiple cycles are done in one measurement. **Right:** A typical shape of a cyclic voltammogram. E_{pa} and E_{pc} are the anodic and cathodic peak potentials. If the peaks show symmetry, the redox reaction can be assumed reversible. For (quasi)-reversible reactions the redox potential ($E_{1/2}$) can be calculated with **(3)**[15].

$$E_{1/2} = \frac{E_{pc} + E_{pa}}{2} \quad \textbf{(3)}$$

2.2. Redox flow batteries

The chemical principles of a redox flow battery (RFB) are the same as in a regular battery: Electricity is stored electro-chemically by changing the oxidation states of the active materials. In a RFB these active materials are all soluble species, usually dissolved ions. A typical setup of a RFB is shown in Figure 3 [16]. It consists of two reservoirs for storing charged/discharged electrolytes, pumps for pumping the electrolyte and an energy conversion system. This energy conversion system consists of 2 half-cells and an ion exchange membrane to separate the electrolytes. Each electrolyte is pumped through one of the half cells, where the electron transfer happens at an inert electrode (usually some form of carbon). The electrolytes usually consist of redox active species and a high concentration of a supporting electrolyte to improve the conductivity, and hence reduce the solution resistance. Depending on the electrolyte, also acids, bases or pH buffers can be added, to improve the stability of the active species.

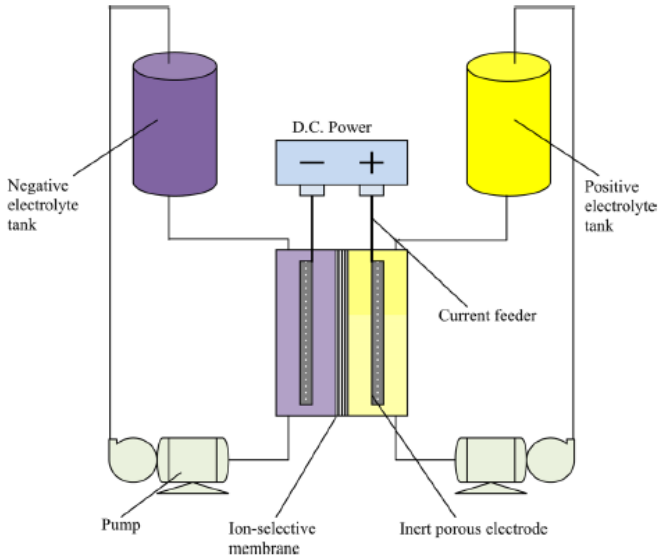

Figure 3. Schematic representation of a redox flow battery (RFB). Figure taken from "Progress in Flow Battery Research and Development"[16] with permission from author

The most developed RFB is the All-vanadium RFB[16, 17], which uses the V(II)/V(III) and V(IV)/V(V) couples as electrolytes. All ions are positive (V^{2+}, V^{3+}, VO^{2+}, VO_2^{+}), and can therefore be separated with an anion exchange membrane. The All-vanadium RFB battery is one of the few RFB's that has been used for large scale applications. However, the high costs and toxic materials prevented widespread applications[18].

There are however some limitations when it comes to choosing the electrolytes for a RFB:

- The redox active compounds must be soluble under the conditions of the cell (e.g. low/high pH or raised temperature) and should not undergo irreversible reactions under these conditions. Preferably the compounds have to be soluble at high concentrations to obtain a sufficiently high power density, which is defined as kW per kg of system or kW per L electrolyte.
- Both half cells must be separable. This means that a suitable membrane must be available to separate the two half cells. For the electrolytes this means usually that the ions must all be either positive or negative, so they can be separated by an ion exchange membrane that allows transport of counter-ions.

- A problem that will always occur is crossover contamination[19], which is the diffusion of active species across the membrane. Membranes with a high selectivity are therefore preferred. In general cation exchange membranes are more selective than anion exchange membranes [20, 21]. Along this reasoning negatively charged redox species would therefore be preferred.
- Some crossover will always occur, therefore the redox species should not undergo irreversible reactions with each other.
- Both half-cells must be able to operate at the same pH. Using a setup with regular monopolar ion exchange membranes would result into Donnan dialysis[22], which eventually makes both pH levels the same again. It is possible to operate two half cells at different pH levels by using a bipolar membrane. This will however result in a higher internal resistance and therefore higher losses.
- The half-cell potential of both redox species should be within the water splitting window, see Figure 4. If this is not the case, the redox reaction would not occur since H_2 or O_2 would be produced instead.

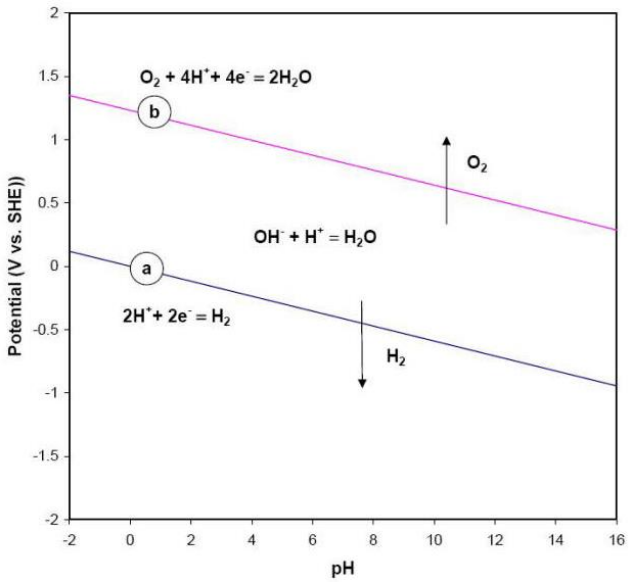

Figure 4. A graph of the half-cell potential of the water splitting reactions vs the pH. If the half-cell potential of an aqueous redox reaction falls outside these two lines, it will not occur and water will react instead. (*Source of image is unknown*)

2.3. The Seebeck coefficient

The driving force of the system developed in this thesis is the Seebeck effect. In the next two sections the Seebeck coefficient will be explained in depth. The first section will mainly focus on the thermodynamic background, the second on the effect of concentration and additives on the Seebeck coefficient.

2.3.1. Thermodynamics of the Seebeck coefficient

The Gibbs free energy can be expressed in enthalpy and entropy with the following relation:

$$\Delta G = \Delta H - T\Delta S \qquad \textbf{(4)}$$

Combining equation **(2)** and **(4)** leads to:

$$E = \frac{T\Delta S - \Delta H}{nF} \quad \textbf{(5)}$$

The temperature dependence of the cell potential is then expressed like this:

$$\alpha = \left(\frac{dE}{dT}\right) = \frac{\Delta S}{nF} + \left(\frac{T\left(\frac{d\Delta S}{dT}\right) - \left(\frac{d\Delta H}{dT}\right)}{nF}\right) \quad \textbf{(6)}$$

Here α is the Seebeck coefficient of the redox reaction in V/K. In **(6)** Δ represents the change due to reaction and d is used for a derivative, e.g. (dΔS/dT) is the derivative of the reaction entropy to the temperature.

α can be expressed in terms of the reaction heat capacity and reaction entropy with the following relations, assuming constant pressure (dP = 0):

$$\left(\frac{\partial \Delta S}{\partial T}\right)_P = \frac{\Delta C_P}{T} \quad \textbf{(7)}$$

$$\left(\frac{d\Delta H}{dT}\right) = d\Delta S = \left(\frac{\partial \Delta S}{\partial T}\right)_P dT + \left(\frac{\partial \Delta S}{\partial P}\right)_T dP = \int \frac{\Delta C_P}{T} dT \quad \textbf{(8)}$$

Unfortunately there is little data available on the heat capacity of dissolved species, so little can be said about the magnitude of the ΔC_P term[23]. However, the two terms are of opposite sign and most likely cancel each other out. Hammond and Risen calculated the magnitude of this term for a MnO_4^{2-}/MnO_4^- couple and came to the conclusion that C_P terms have only a small effect (up to 8% of ΔS)[23]. If we assume that ΔS and ΔH are indeed almost independent of temperature, the expression simplifies to (which is what most articles in literature report [13, 23, 24]):

$$\alpha = \frac{\Delta S}{nF} \quad \textbf{(9)}$$

For a simple redox reaction such as $A + ne^- \leftrightarrows B$, ΔS is expressed as[12]:

$$\Delta S = (S_B + S_B^*) - (S_A + S_A^*) - n\overline{\overline{S_e}} \quad \textbf{(10)}$$

Here S_A and S_B are the molar entropy of the ions. S_A^* and S_B^* are the Eastman entropy of transport and $\overline{\overline{S_e}}$ is the total transported entropy of the electrons in the electrode. $\overline{\overline{S_e}}$ can usually be neglected, since it usually only contributes 1% of the total entropy[24, 25]. The contributions of S_A^* and S_B^* are also relatively small compared to the molar entropies, for example for the $Fe(CN)_6^{3-}/Fe(CN)_6^{4-}$ redox couple this is 10 µV/K [25] which is only 1% of the total Seebeck coefficient. The expression then simplifies to:

$$\alpha \cong \frac{S_B - S_A}{nF} \quad \textbf{(11)}$$

This simple expression can be used to predict the Seebeck coefficient for various electrolytes. However for many ions (e.g. Cr^{2+}, Cr^{3+}, I_3^- or redox active organic molecules), the molar entropy is not available in common databases such as NIST and the CRC-handbook[26, 27] neither could the Seebeck coefficient be predicted by software, such as OLI Stream analyzer or ASPEN Properties. We are currently looking into

predicting the entropy change using molecular simulations, in collaboration with Dr. Remco Hartkamp. At the moment of writing this thesis, no conclusions can be drawn yet.

For dissolved ions, the hydration shell (ordered water molecules around the ion) has a large contribution on the entropy. When the magnitude of a charge increases, the hydration shell becomes bigger. Using this, we developed a theory (Figure 5) to predict the sign of the Seebeck coefficient for simple reactions where only the charge of a compound changes.

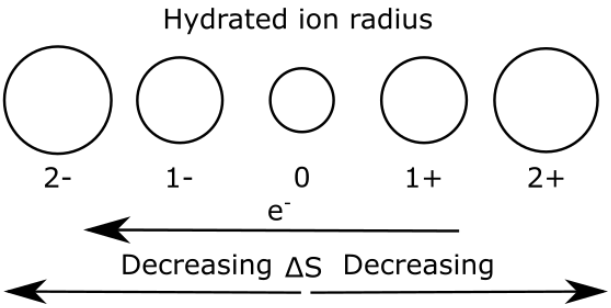

Figure 5. Illustration to show how the entropy changes for a simple redox reaction. If a neutral specie or anion gains an electron, the system becomes more ordered (the hydration shell becomes bigger). Therefore the entropy change is negative. The opposite happens for cations, where the entropy change is positive.

Using this theory we can predict:

- for redox couples with just anions or neutral species($A^{n-} \rightleftharpoons A^{(n-1)-} + e^-, n \geq 1$), α is negative.
- for redox couples with just cations or neutral species($A^{n+} + e^- \rightleftharpoons A^{(n-1)+}, n \geq 1$), α is positive.

The theory agrees with literature data for many simple redox couples such as V^{2+}/V^{3+} and Fe^{2+}/Fe^{3+},[24] but also for more complex couples such as $Fe(CN)_6^{3-}/Fe(CN)_6^{4-}$ and Cu-pyridine complexes[23].

Using this information we can calculate, or predict the Seebeck coefficient for many different ions. For more complex reactions such as $I_3^- + 2e^- \rightarrow 3I^-$ it remains tricky to predict the Seebeck coefficient, because the thermodynamic data is not available and the relation of Figure 5 no longer holds.

2.3.2. Effect of concentration and additives

It is possible to influence the Seebeck coefficient of an electrolyte by changing properties, such as the concentration or by adding liquids to the electrolyte.

The effect of the concentration on the Seebeck coefficient is not really useful in practice. It is almost always desired to work at saturated concentrations to reduce internal resistance and to allow for bigger conversions. deBethune *et al.* did an analysis of the effect of concentration on the Seebeck coefficient, here are two examples of the effects[24]:

- By changing the molarity of $CuSO_4$ from 0.08 to 1.4 mol/L for a copper/copper sulfate electrode, the Seebeck coefficient changed from +0.64 to +0.75 mV/K.
- When changing the normality of Chlorine from 0.001 to 1.0 for a Ag/AgCl the Seebeck coefficient changed from +0.77 to +0.250 mV/K.

In a review by Quickenden and Mua[11] a wide range of Seebeck coefficients of $Fe(CN)_6^{3-}/Fe(CN)_6^{4-}$ are reported for various concentrations, ranging from 1.0 to 7.4 mV/K (the sign of the value was not reported). This effect seems too large and is likely a mistake in reporting. All articles of this topic are either very old, or show doubtful results. Therefore the effect of concentration on the Seebeck coefficient will be checked experimentally as well. This is reported in section 4.1.4.

Perhaps more interesting, is the effect of additives on the Seebeck coefficient. This phenomena was reported recently by Kim *et al.* [28]. Kim *et al.* report Seebeck coefficients for $Fe(CN)_6^{3-}/Fe(CN)_6^{4-}$ in fifteen different organic-water solutions. The strongest effect was observed for methanol: for a 20wt% methanol solution the Seebeck coefficient decreased from -1.43 to -2.9 mV/K.. The effect of ethanol on the Seebeck coefficient of $Fe(CN)_6^{3-}/Fe(CN)_6^{4}$ and I^-/I_3^- will be determined experimentally in Chapter 4.1.4.

2.4. The Thermal regenerative electrochemical cycle

The Seebeck effect in batteries can be used to convert thermal energy into electricity, which is done in the thermal regenerative electrochemical cycle (TREC)[13]. A cycle can be constructed, where a battery is discharged at T_1 and charged back at T_2. If the charging voltage is lower at T_2 than the discharging voltage at T_1, net energy is produced by the voltage difference originating from the Seebeck effect.

Previously only the Seebeck coefficient of a half-cell was discussed. A battery is a combination of 2 half-cells. The Seebeck coefficient of a battery or full cell (α_{full}) can be obtained by subtracting the Seebeck coefficient of the negative electrode (α_2) from the positive electrode (α_1):

$$\alpha_{full} = \alpha_1 - \alpha_2 \qquad (12)$$

At which temperature the charge or discharge happens depends on the system:

- If $\alpha_1 > \alpha_2$, α_{full} is positive (see Figure 6). That means $\Delta E_{hot} > \Delta E_{cold}$ therefore one needs to charge at low and discharge at high temperature.
- If $\alpha_1 < \alpha_2$, α_{full} is negative. That means $\Delta E_{hot} < \Delta E_{cold}$ therefore one needs to charge at high and discharge at low temperature.

Let $\Delta E = \Delta E_{hot} - \Delta E_{cold}$, where $\Delta E > 0$. The work performed by the TREC would be defined by (Figure 7):

$$W = \Delta E * It = \alpha_{full} * \Delta T * It \qquad (13)$$

Here W is the work performed in Joule, ΔE is the potential difference between the cold and hot battery due to the Seebeck effect. I*t is the state of charge which defines how much of the battery is (dis)charged. ΔT is the temperature difference between the hot and cold cell. The system should have a **current efficiency** of almost 100%. For example, a system with 80% current efficiency, wastes 20% of the input energy for charging. This energy loss is most likely higher than what can be recovered with the TREC.

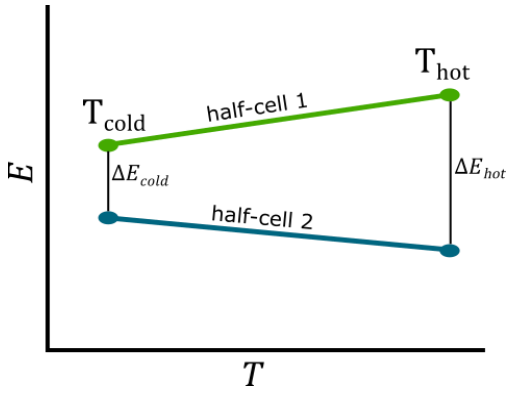

Figure 6. Potential vs temperature for a positive α. For a positive α, the potential difference will be higher at a higher temperature. Half cell 1 and half cell 2 indicate the half-cell of the positive and negative electrode respectively.

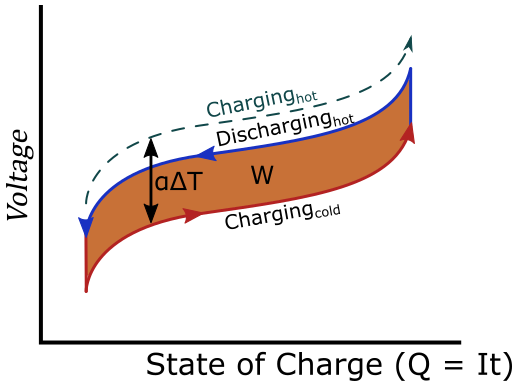

Figure 7. The voltage plotted vs the state of charge for the TREC. The dashed line indicates what the voltage would be if the temperature did not change, it is shifted by αΔT. The brown area in this figure is the performed work by the TREC.

Current Efficiency

The current efficiency, also called Faradaic or Coulombic efficiency, describes the efficiency in which electrons are transferred in an electro-chemical reaction. It is defined as:

$$\eta_C = \frac{Q_{discharge}}{Q_{charge}} * 100\% \qquad \textbf{(14)}$$

A common example of charge losses is the self-discharge of a battery, which reduces the charge available for discharge.

Now we shift our focus from a regular battery to a flow battery (Figure 8): A redox reaction is happening at T_1 in one cell, and the reverse reaction at T_2 in the other cell. Both reactions happen at the same rate. The electrolytes are circulated between both cells, through a heat exchanger, which results in a continuous system. The heat to power efficiency of an ideal thermogalvanic cycle with a perfect heat exchanger is defined in the following way:

- The heat put into the system is $T_H\Delta S$ at the hot cell (this is a result from the endothermic reaction which occurs in the hot cell)
- The energy that is converted is $\Delta G_H - \Delta G_C = (T_H - T_C)\Delta S = \Delta T \Delta S$

$$\eta = \frac{(T_H - T_C)\Delta S}{T_H \Delta S} = 1 - \frac{T_C}{T_H} \qquad \textbf{(15)}$$

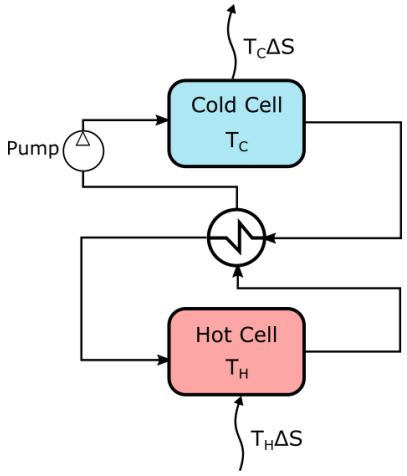

Figure 8. Schematic representation of a TREC based on flow batteries, operating at temperatures T_C and T_H with a heat exchanger and a pump.

Equation **(15)** is the same as the Carnot efficiency mentioned in Chapter 1. However, a real world heat exchanger does not work perfect. Also energy losses (e.g. electrical losses or energy consumption by pumps) need to be taken into account. Then equation **(15)** transforms into:

$$\eta = \frac{\Delta T \Delta S - Q_{loss}}{T_H \Delta S + Q_{HX}} = \frac{\Delta T\ \alpha_{full}\ nF - Q_{loss}}{T_H\ \alpha_{full}\ nF + Q_{HX}} \qquad \textbf{(16)}$$

There Q_{loss} represents the losses of energy from various sources (in Joules). Q_{HX} is the heat required raise the temperature of the hot cell to T_H after the heat exchanger. It is desired to have a Seebeck coefficient which is as high as possible. A big α results into having a larger power output compared to the losses and will therefore approach the Carnot efficiency.

If E_{OC} is the open-circuit voltage difference between the hot and cold cell, E_{loss} voltage losses from various sources and R_{int} the internal resistance (in $\Omega\ m^2$) of the system. Then the maximum power density of the TREC is defined as (for the derivation of equation **(17)**, see Appendix A):

$$P_{max} = \frac{(E_{OC} - E_{loss})^2}{4R_{int}} = \frac{\left(\alpha_{full}\Delta T - E_{loss}\right)^2}{4R_{int}} \qquad \textbf{(17)}$$

So in order to have a high performance system, the E_{loss} and R_{int} have to be minimized. E_{OC} should be maximized as much as possible, the Seebeck coefficient should therefore be as high possible. ΔT should also be as big as possible.

Using the theories of this chapter, some more criteria are presented below on which the system has to be selected:

- Seebeck coefficient has to be as high as possible. This can be done by combining two redox couples with large Seebeck coefficient of opposite sign.
- The redox couples should have low or no overvoltage, to minimize E_{loss} as much as possible.

- R_{int} should be as low as possible. A high concentration of current carrying ions is therefore required, and the redox couples should be stable in this.
- The current efficiency of the redox reactions should be almost 100%, otherwise losses will be too big.
- All materials should be stable on a wide temperature interval (at least 10 - 60°C so a Carnot efficiency of 15% is reached).

2.5. Literature examples

Before discussing the design of this thesis, first two examples from literature will be discussed. After a brief introduction into the reported systems, the observations and recommendations of the researchers will be presented.

2.5.1. Lee, *Nature Communications* 2014[13]

This article reports a regular battery with two solid electrodes, consisting of copper-hexacyanoferrate (CuHCF), and copper (Cu/Cu^{2+}) negative electrode (Figure 9). $Cu(NO_3)_2$ and $NaNO_3$ are added as supporting electrolyte. The half-reactions during discharge are:

$$Na^+ + Cu_{1.5}Fe(III)(CN)_6 + e^- \rightarrow NaCu_{1.5}Fe(\text{II})(CN)_6$$

$$Cu \rightarrow Cu^{2+} + 2e^-$$

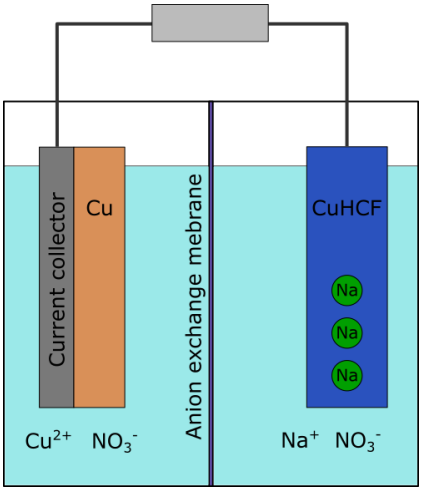

Figure 9. Schematic representation of the system reported by Lee *et al*[13]. The grey box indicates multiple operations (discharging/charging).

This system has a Seebeck-coefficient of -1.20 mV/K. Therefore the system needs to be charged at high and discharged at low temperature to gain energy. The system is more efficient than the best thermoelectric techniques (see Chapter 1). A 3.9% heat to power efficiency was reported for charging/discharging at 10 and 60 °C without any heat recuperation, this is 26% of the Carnot efficiency for this temperature interval. Also stable cycling was reported, with the heat to power efficiency dropping only 0.2 % after 40 cycles.

The criteria's on which Lee *et al.* selected this system are the following:

- Fast kinetics
- High charge capacity
- High α coefficient
- Low-heat capacity

Fast kinetics, high α and low heat capacity are the most important for our system. Fast kinetics result in a lower resistance and overpotential and thus smaller losses. High α coefficient makes the system less prone to losses, as discussed before. And a low heat capacity makes sure more thermal energy is recovered as electricity, instead of only heating and cooling the system.

2.5.2. Hammond and Risen, *Solar Energy* 1979[23]

Hammond and Risen reported a system closer to the desired design of this thesis. They reported various copper and iron based electrolytes. To test these electrolytes, a single cell was built, and the temperature dependence of the potential was reported, see Figure 10A. Based on the high reaction entropy (linearly related to the Seebeck coefficient) they paired a copper-ammonia based electrolyte, and hexacyanoferrate:

$$Cu(NH_3)_4^{2+} + e^- \rightleftharpoons Cu(NH_3)_2^{+} + 2NH_3$$

$$Fe(CN)_6^{4-} \rightleftharpoons Fe(CN)_6^{3-} + e^-$$

Apart from these two electrolytes, NH_4Cl and K_2SO_4 were added to conduct current. A $BaSO_4$ precipitate membrane was added to separate the two electrolytes. However, after running the cell for 5.5 hours, a sudden sharp peak (200%) in the resistance was observed. The peak was caused by $Cu_2Fe(CN)_6$ precipitating on the membrane, observed by a color change. An idea for a continuous heat recovering system was also presented by Hammond and Risen (Figure 10B). However, the precipitation and poor solubility of reactants and large internal resistance of the system prevented them from developing it.

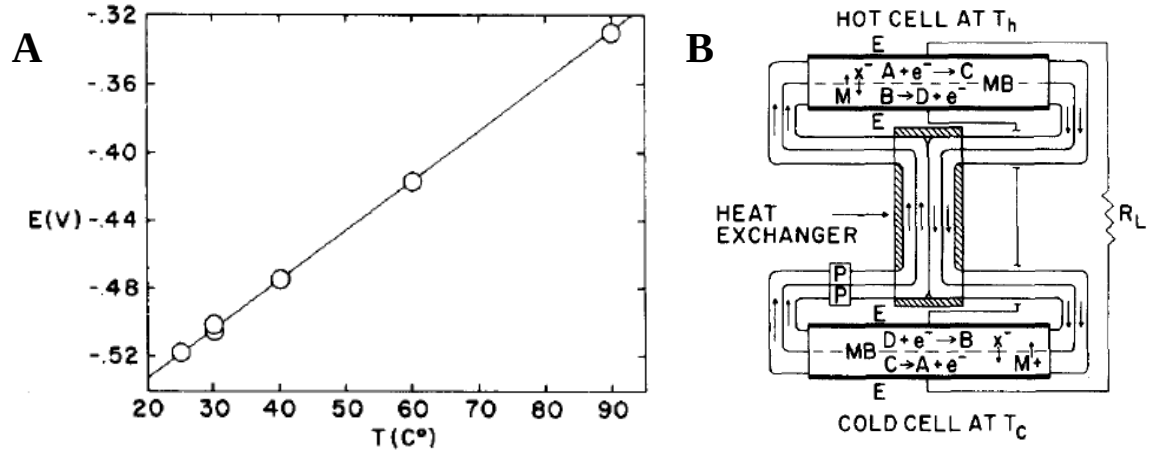

Figure 10. Figures from Hammond and Risen [23], Solar Energy 1979 **A** The full cell potential plotted versus the temperature. **B** Schematic representation of a continuous heat recuperation system, with the reactions $A + e^- \leftrightarrow C$ and $B \leftrightarrow D + e^-$. The voltage difference between the hot cell operated at T_h and the cold cell operated at T_c allows one to generate energy. P represents a pump.

Despite the highly predicted efficiencies of the system (50% of Carnot efficiency at max power, assuming 100% heat exchange efficiency), the system by Hammond and Risen received little attention and was cited only 7 times [11, 13, 29-33]. Unfortunately none of these articles continue on the proposed system and the development of the system stopped where it started in 1979.

In their conclusion, Hammond and Risen state six requirements for a successful cell reaction but these have already been mentioned previously in section 2.2 and 2.4.

2.6. The design of the setup of this thesis

As was already mentioned in the introduction, in this thesis a system will be designed for low-grade waste heat recovery, using the TREC with flow batteries. The design needs to meet certain specifications in order to work. For the electrolytes and membranes these have already been discussed in 2.2 and 2.4.

When designing the other parts of the cell, the following aspects have to be taken into account as well:

- When iron parts should be protected, when using $Fe(CN)_6^{3-}/Fe(CN)_6^{4-}$ to prevent formation of Prussian blue[34].
- All materials should be stable and not undergo phase change on a large temperature interval (at least 0 – 80 °C)
- On this temperature interval the materials should be resistant to used pH and possible corrosive electrolytes
- The materials in contact with the electrolyte should not conduct electricity(apart from the electrode)

2.7. Research goals and questions

In this paragraph the research goals are discussed, and the research questions are presented.

The goal of this thesis is to design a low grade heat recovery system, based on the TREC using flow batteries. This consists of selecting electrolytes, designing the parts and items required to run the system.

The main research question is:

What is the efficiency of a heat to power system using the thermally regenerative electrochemical cycle, based on redox flow batteries?

The sub questions are:

- *Which electrolytes are most suitable for such a system?*
- *What is required for a system with net gain?*
- *What are the main causes for energy losses?*
- *Can we experimentally validate the heat to power efficiency?*

3. Experimental

This chapter will display the experimental techniques that were performed and the amount of the chemicals that were used. First the setup and preparation of electrolytes for measuring the Seebeck coefficient will be discussed. Then the synthesis method of Alloxazine carboxylic acid (ACA) will be shown. This is followed by the building of the flow cell. After that the experimental setup for doing experiments with one flow cell will be shown. Finally it will be explained how the ASPEN Plus model was created. The suppliers and purities of all the chemicals are in Appendix F.

3.1. Determining the Seebeck coefficient

The selection of the final electrolytes was done on the basis on the Seebeck coefficient. For the following three redox couples, the Seebeck coefficient was measured:

- $Fe(CN)_6^{3-} + e^- \rightleftharpoons Fe(CN)_6^{4-}$
- $I_3^- + 2e^- \rightleftharpoons 3I^-$
- $ACA + 2H^+ + 2e^- \rightleftharpoons ACA\text{-}2H$

First the measuring setup will be explained. Then the electrolytes of the above redox reactions will be discussed.

The setup for measuring the Seebeck coefficient:

As was mentioned in section 2.3.3, a setup had to be designed in order to measure the Seebeck coefficient. Two beakers at different temperatures need to be in ion-conductive contact, while not influencing the temperature of the other beaker.

The obvious solution is connecting both beakers with a long salt bridge. Common salt bridges, such as filter paper soaked in a salt solution or glass tube filled with salt solution jellified by Agar, are however not very practical for our application. A long piece of paper would probably have a too high resistance which will make the voltages too high to be measured by the potentiostat. Also a long string of paper is difficult to handle. The Agar has a relatively low melting point (74 to 97 °C)[35], which in a heated beaker could destroy the salt bridge.

A new piece of equipment was therefore designed: a 30 cm long glass U-shaped tube with two porous filters at the ends and an opening at the top (for the blueprint see appendix G). The tube can be filled/emptied with conducting salt solution from the top, and the porous filters prevent the electrolytes from entering the salt bridge. The porous filters only worked if the concentration of ions in the salt bridge and beakers was the same, otherwise osmosis occurred. The measuring setup for the Seebeck coefficient is shown below in Figure 11.

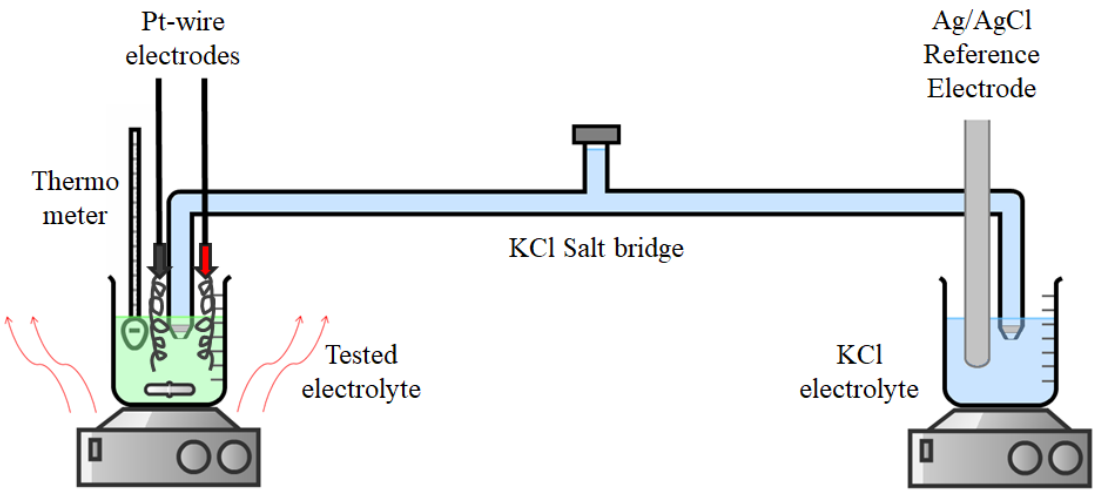

Figure 11. Schematic representation of the setup used for measuring the Seebeck coefficient. On the left is a heated beaker with two Pt-wire electrodes, a thermometer and a magnetic stirring bar. On the right is a beaker at room temperature with a Ag/AgCl electrode. These two beakers are connected with a salt bridge of 30 cm long, which has two porous filters at the ends to separate the tested electrolyte from the KCl electrolyte. The potential difference is measured between the work electrode (Pt-Wire) and the Ag/AgCl reference electrode.

Preparation of the electrolytes:

The electrolytes were prepared in the following manner: The solid compounds of interest were weighed and added to a 50 mL flask. KCl was added to make the K^+ concentration of 1 mol/L. Demineralized water was added until the volume reached 50 mL. All compounds were dissolved by shaking the flask and stirring by spatula. The salt bridge was filled with a KCl solution with the same concentration as that of the electrolytes, to prevent osmosis through the porous filters.

Hexacyanoferrate can undergo an irreversible reaction with iron to form Prussian blue. In the first experiment, the stainless steel thermometer was corroded due to this reaction. Afterwards the thermometer was protected by a finger of a safety glove filled with water. The thermometer was calibrated with ice water and boiling water. The thermometer was still working properly, so it can be assumed that the Prussian blue did not damage the sensor.

For cyclic voltammetry it is required to have both the oxidizing and the reducing agent of a redox couple in the mixture. Since the synthesized ACA compound only consists of the oxidizing form, it had to be partly converted. 20 mL of the ACA solution was reduced by a $K_4Fe(CN)_6$ solution with a current of ~2.80 mA (this was the highest possible current) for 9.5 hours to receive equimolar concentrations of ACA and ACA-2H. A photo of this setup can be found in Appendix E.

The Seebeck coefficient was calculated by performing cyclic voltammetry (CV) at various temperatures. Two Pt-wires, pretreated in sulfuric acid were used as working and counter electrode. A refillable Ag/AgCl electrode from Q-I-S B.V. was used as reference electrode. The potential difference was measured between the reference electrode and the working electrode. All electrodes were connected to an Iviumstat COMPACTSTAT (800 mA) and the voltages were read out from the computer.

The procedure for measuring the Seebeck coefficient was as follows: A CV-scan consisting of 4 cycles was done then the electrolyte was heated 5 degrees and this was repeated from 20 to 55 °C. The Seebeck coefficient was then calculated by linear regression in Python.

The weighed amounts for the experiments are shown in the Table 2 below:

Table 2. Weighed amounts of material of the electrolytes, during the Seebeck coefficient measurements.

Experiment				
$Fe(CN)_6$	$K_3Fe(CN)_6$	$K_4Fe(CN)_6 \cdot 3H_2O$	KCl	Demi-Water
	1.745 g	2.144 g	1.131 g	50 mL
I^-/I_3^-	KI	I_2	KCl	Demi-Water
	0.098 g	0.015 g	3.727 g	50 mL
ACA	ACA (50% reduced later)	KOH (45 w/v)	KCl	Demi-Water
	0.646 g	7.25 mL	3.342 g	50 mL

3.2. Synthesis and Characterization of ACA

Alloxazine Carboxylic Acid (ACA) was prepared according to a previously reported synthesis method[36]. A brownish suspension of 7.51 g (50 mmol) 3,4-Diaminobenzoic acid stirred in 425 mL of acetic acid was prepared first. 3.4 g (55 mmol) of Boric acid and 7.53 g (53 mmol) of Alloxane monohydrate were added to the solution. The reaction was stirred for 4.5 h at room temperature. During the reaction, the color of the mixture went from dark brown to dark yellow to finally a green yellowish suspension. After that the product was filtered off and washed, first with acetic acid, then with diethyl ether, water and finally diethyl ether.

From the ^{1}H-NMR spectra in Appendix D it can be concluded that indeed pure ACA was synthesized. However, the peak around 1.91 (which is characteristic for acetic acid in DMSO-d6 [37]) shows that there is contamination of acetic acid. To remove most acetic acid from the ACA, the compound was further dried in air for 2 days.

3.3. Building the flow cell

The flow cell was designed for this thesis. The design is based on a smaller flow cell created by David Vermaas[38]. The smaller flow cell has a circular electrode with a radius of 1 cm and was scaled up to 5 cm in the design. 3D-drawings of the flow cell were created using Autodesk Inventor. All the sizes and measurements are displayed in Appendix G.

The design of the flow cell was done in parallel to choosing the electrolytes. The materials therefore had to be resistant to a large amount of chemical conditions (e.g. Alkaline, acidic or presence of bromine) at a wide temperature range. The ideal material for this is Teflon, which is resistant to almost everything and has a maximum operating temperature of 260 °C[39]. Teflon is a soft material, which is not suitable for thin (< 3 mm) parts. As second material, a polyamide (PA2200) was used.

The flow cells contain three designed parts:

- PA2200 (a polyamide based plastic) 3-D printed spacer, manufactured by Oceanz 3D printing. Before building the flow cell it was sanded to smoothen the rough surface. (see Figure 12)
- Teflon Back plate. Milled from a plate of Teflon by DEMO of the TU Delft. (see Figure 12)

- Aluminum support plate. Created by drilling multiple holes in an aluminum plate by DEMO of TU Delft. Teflon is a very soft material. In order to prevent it from deforming from the force of the screws, an aluminum plate was added to spread the force more evenly across the plates.

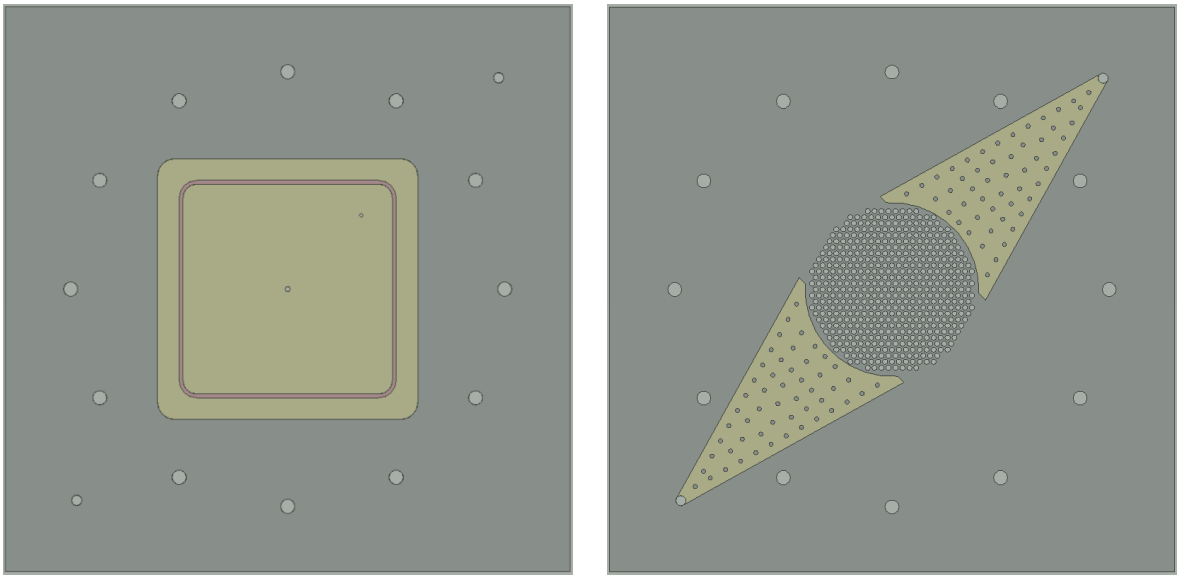

Figure 12. Screenshot of Autodesk designs of the flow cell parts. **Left:** Design of the Teflon back-plate. The biggest circles indicate the screw holes, the outer two circles on the diagonal are for the fluid inlet and outlet. The two smaller circles on in the middle are holes for wires, to have electrical contact. The red circle is a groove for an O-ring, to protect the wires from short circuiting and prevent leakage. Yellow indicates the compartment for the electrode. Pink is the O-ring groove. **Right:** Design of the PA2200 spacer, Electrolytes flow diagonally up, where they meet a circular hole. Here, there is contact with the electrode and membrane. Finally the electrolytes flow up and out the cell. Along the electrolyte flow area, there are little pillars to keep the membrane in place. In the middle, there is a porous plate to keep the membrane in place, while still keeping contact with electrolyte. Yellow indicates the compartment for the electrolyte to flow.

In both Teflon back plates, graphite foil electrodes were placed. These electrodes were connected with two wires each through two holes in the back plate. To prevent short circuiting and leakages a rubber O-ring was added, to seal the wires from any fluid coming in. This O-ring was custom created by super-gluing two ends of an O-ring cable together. On the top of the back plate, there is a hole for the reference electrode to measure the outflow. The Ag/AgCl electrodes were the same as in chapter 3.1, and were also sealed with O-rings and a custom made Teflon screw (see Appendix G) to prevent air coming into the electrolytes.

The two sides were separated by a FKB-PK-130 cation exchange membrane from FuMaTech. All parts were pressed together with 300 µm thick Silicone gaskets between the back plates and spacers and the spacers and membrane. Finally everything was screwed together with M12 steel screws. Figure 21 shows a scheme of the assembled flow cell.

3.4. Experiments with the cell

To perform the cell experiments, the flow cell was connected with 8 mm (outer diameter) PTFE tubes to a Masterflex L/S peristaltic pump and two 1 L glass bottles with electrolytes. All tubes were connected using polypropylene connector pieces from EM-Technik. In the caps of the glass bottles two 8mm holes

were drilled for the inflow and outflow and a 2 mm hole for a smaller tube which allows built up pressure to be released.

The current and the potential were measured/applied with a Compactstat (maximum current of 800 mA) from Ivium technologies. The electrodes were attached with the following combinations:

- Working electrode: I^-/I_3^-
- Counter electrode: $Fe(CN)_6^{3-}/Fe(CN)_6^{4-}$
- Sense electrode: $Fe(CN)_6^{3-}/Fe(CN)_6^{4-}$
- Reference: I^-/I_3^-

The temperatures were measured by K-type thermocouples from TC-direct. To measure the in- and outflow temperature of the electrolyte, the thermocouple was pushed through a T-piece stuffed with a PTFE disc (see Figure 14). The stainless steel thermocouple was protected by a layer of glue to prevent Prussian blue formation by hexacyanoferrate. The temperatures were read out by a NI-9213 from National Instruments, and converted into data files with LabVIEW.

The electrolytes were heated by looping the PTFE tube three times through a heating bath from Julabo. To reduce heat dissipation from the tubes, isolation tubes from Gamma were used to isolate the tubes between the heat bath and flow cell. Since the setup requires many different parts, tubes and cables, it was decided to design a custom table. The table (Figure 13) was built by Item Industrietechnik.

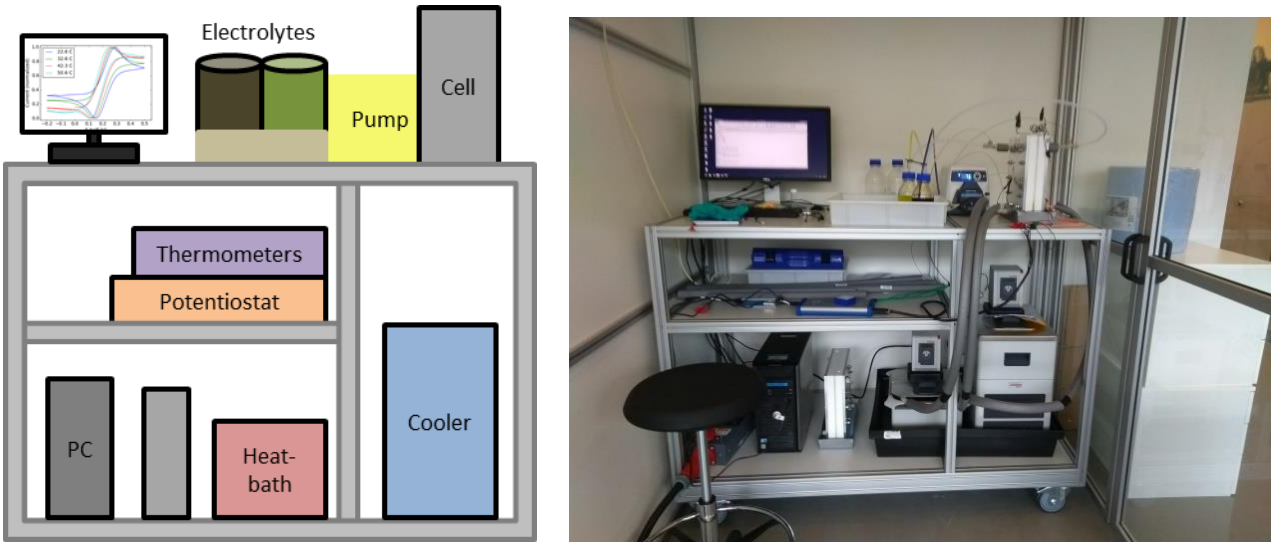

Figure 13. Photos of the flow cell setup. **Left:** Schematic representation of the flow cell setup **Right:** Picture of the setup, the flow cell is connected to the heat bath with isolated tubes. Right of the pc is the second flow cell.

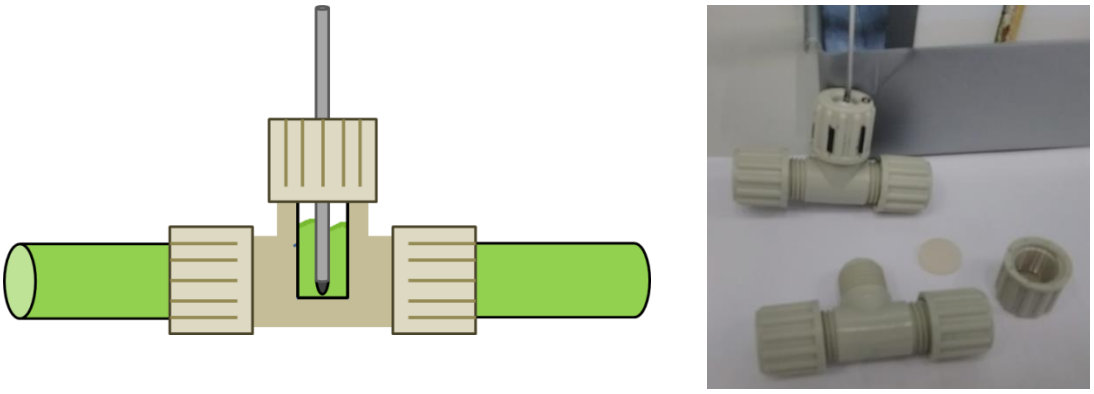

Figure 14. **Left:** Schematic representation of temperature measuring setup with a T-junction. The green color indicates the electrolyte, the grey stick the thermocouple. The T-piece is made transparent in the center to show how the thermocouple touches the electrolyte. **Right:** Photo of the thermocouple setup. On the top is the assembled piece, below are the 3 separate parts

For the measurements itself, the pump was always set on 75 rpm, which translates to 1 mL/s[40]. The compositions of the electrolytes are shown in Table 3.

Table 3. Compositions of the electrolytes, and the weighed amounts for 1 Liter of electrolyte.

$Fe(CN)_6^{3-}/Fe(CN)_6^{4-}$ electrolyte			I^-/I_3^- electrolyte		
Chemical	Molarity (mol/L)	Weighed amount (g)	Chemical	Molarity (mol/L)	Weighed amount (g)
$K_3Fe(CN)_6$	0.1	32.95	I_2	0.1	25.15
$K_4Fe(CN)_6 \cdot 3H_2O$	0.1	42.19	KI	0.3	49.83
KCl	0.3	22.40	KCl	0.7	52.20

3.5. ASPEN Plus model

The TREC system was simulated with an ASPEN Plus model (see Figure 15). The thermal properties of all electrolytes were assumed to be that of water, since the data for heat capacity was not available for the solutions. The composition of the streams was identical to those reported in Table 3 in the previous section.

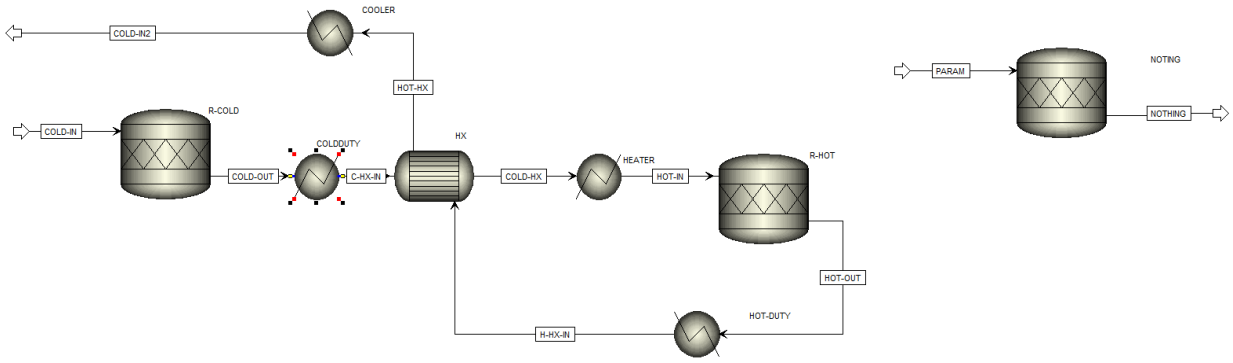

Figure 15. Screenshot of the ASPEN Plus flow sheet

The TREC was modelled as two stoichiometric reactors, one at high temperature and the other at low temperature. To improve calculation speed, the system was modelled as an open loop. It was constantly

checked to see if the loop was indeed correct. The two outflow streams of the reactor were pumped to two heaters, which add the heat of reaction to the stream and then flow through a heat exchanger. After the heat exchanger the streams go to a heater and cooler to be adjusted to the temperatures of the reactors. The duty of the heater of the hot side is used as an energy input to the system.

On the right side of Figure 15 one can see an additional reactor. This reactor is a dummy and is only used to store parameters (in the form of mole flows) which ASPEN does not have itself, such as current density or electrode area.

All the electrochemical calculations are done through calculator blocks. These calculator blocks also set the conversion and heat of reaction of the reactors, and calculate the power and efficiency of the system. Finally, various sensitivity analysis blocks were used to study the effect of current density and electrode area on the efficiency and electrical power.

4. Results and Discussion

This chapter is divided into three parts. First the selection procedure and characterization of the electrolytes will be discussed. Then the design of the flow cell will briefly be explained, and the results of experiments with the flow cell shall be presented. Finally, a numerical approach to the design will be taken using a model created with ASPEN Plus.

4.1. Selecting the Electrolytes

The selection of the electrolytes happened in three steps: First a literature study was done, from which a database of 44 different RFB systems was created (see Appendix B). From these 44 systems the best electrolytes were then selected on basis of the criteria mentioned previously in chapter 2.6. Finally, the chosen electrolytes were characterized experimentally.

4.1.1. Literature Study

When starting the project, it seemed an obvious choice to use the most developed RFB system as a basis of our heat to power design. This system is the All-Vanadium Redox flow battery (V-RFB), which is driven by the following two redox reactions at low pH:

$$V^{3+} + e^- \rightleftarrows V^{2+}$$

$$VO^{2+} + H_2O \rightleftarrows VO_2^+ + 2H^+ + e^-$$

After doing some research on this system, it appeared to be unusable for our design. This is because the operating range of the V-RFB is 10 – 40 °C[41] (or up to -5 to 50 °C with added stabilizers[41-43]). This small temperature window is a result of an irreversible precipitation reaction that occurs above 40 °C:

$$2\,VO_2^+ + H_2O + SO_4^{2-} \rightarrow V_2O_5 + H_2SO_4$$

An obvious second choice was not available. Therefore it was decided to create a database with possible RFB systems (see Appendix B). Most of these systems were found in the review paper of Skyllas-Kazacos *et al.*[16] and the literature section of Lin *et al.*[44] and Lui *et al.*[45].

It was already discussed in chapter 2, that redox couples need to be at the same pH. In order to visualize better which RFB electrolytes could be combined, the RFB systems were grouped into seven categories:

- Acidic, these aqueous RFB were reported to operate at a low pH
- Alkaline, these aqueous RFB were reported to operate at a high pH
- Neutral, for these aqueous RFB systems, no acid or base was added for operation
- Organic, these are all non-aqueous RFB systems, and run in organic solvents
- Solid, these hybrid-RFB systems have some form of solid electrode, or uncharged metal particles in solution.
- Unfeasible, two RFB systems that use the ions of radioactive elements (Uranium/Neptunium)
- Other, two RFB designs that did not fit any of the above categories, since they run at both low and high pH.

For each system, both half-reactions are reported in the database and if available, the overpotential and temperature operating range as well.

4.1.2. Selection of the electrolytes

The 44 RFBs reported in the database contain of 64 different electrolytes. If these electrolytes are combined, 2016 different full cells could be designed! Therefore an efficient selection procedure is necessary, which will be performed here. (For some more elaboration on why individual RFB systems were excluded, see Appendix C)

The first set of systems was excluded on the basis on the chemical nature, the following exclusion criteria were:

- **Solid material deposition**, a continuous flow battery cell is desired, therefore solid deposition at an electrode is not desired
- **Radioactive electrolytes**, using materials like Uranium or Neptunium is not desired, because of obvious reasons
- **Uses aqueous Mn^{3+} electrolyte**, Manganese(III) ions react with water ($2Mn^{3+} + 2H_2O \rightarrow Mn^{2+} + MnO_2 + 4\ H^+$), and form insoluble MnO_2
- **Uses aqueous Ti^{4+} electrolyte**, the performance of the Titanium couple is seriously compromised by activation polarization[46]
- **Review stated there is no point for further research [16]**, this is the case for $[Ru(bpy)_3](BF4)_2$ which has costly materials and low efficiencies. This is a strong indication the compound will not be useful for the project.

Thirteen RFB systems fell in the categories above. For the second step, any of the 31 remaining RFB systems will be excluded if they do not meet the following process specifications:

- **Electrolytes work on a temperature interval.** The solutions need to be stable at least between 10 – 60 °C. If this cannot be reached, the electrolyte will be unusable for the application.
- **The flow battery has an overpotential smaller than 0.2 V**, If the overpotential is larger than 0.2 V, almost all energy that was converted from heat will be wasted.

For most of the RFB systems, the temperature operating range and overpotential were not reported. If possible, the temperature range was estimated by looking at phase change points of the materials or by the presence of irreversible reactions above or below room temperature. The overpotential was estimated by looking at the I/V curve. If the I/V curve was not linear through the origin, it can be assumed that there is an overpotential. Another thirteen RFBs did not meet the above criteria.

The 18 RFB systems that survived the previous two selections were subject to a final cut. Here the RFB systems were excluded on the basis of practical reasoning (e.g. not working with organic solvents or a system requiring special parts in order to operate). Justification for the exclusion of each system is given in Appendix C. The redox couples of the final RFB systems are displayed in Table 4 below.

Table 4. The final 8 selected RFB systems, with the reactions happening at the anode/cathode during discharging. The red color indicates that the reactions happen in an acidic solution, green indicates an alkaline solution and blue indicates a solution without strong bases or acids.

Name	Cathode reaction	Anode reaction	Reference
Iron-Chromium	$Cr^{3+} + e^- \rightarrow Cr^{2+}$	$Fe^{2+} \rightarrow Fe^{3+} + e^-$	[19, 47, 48]
Vanadium-Iron	$V^{3+} + e^- \rightarrow V^{2+}$	$Fe^{2+} \rightarrow Fe^{3+} + e^-$	[49] [50]
Vitamin B2 based	$ACA + 2e^- + 2H^+ \rightarrow ACA\text{-}H_2$ (ACA = Alloxazine Carboxylic Acid)	$Fe(CN)_6^{4-} \rightarrow Fe(CN)_6^{3-} + e^-$	[44]
All-Soluble All-Iron Aqueous Redox-Flow Battery	$[Fe(TEOA)OH]^- + e^- \rightarrow [Fe(TEOA)OH]^{2-}$ (TEOA = Tri-ethanolamine)	$Fe(CN)_6^{4-} \rightarrow Fe(CN)_6^{3-} + e^-$	[51] [52]
Alkaline flow battery based on coordination chemistry of Fe and Co	$[Fe(TEOA)OH]^- + e^- \rightarrow [Fe(TEOA)OH]^{2-}$ (TEOA = Triethanolamine)	$[Co(mTEOA)H_2O]^- \rightarrow [Co(mTEOA)H_2O] + e^-$ (mTEOA = Methyl-triethanolamine)	[52] [53]
Ferro/ferricyanide polysulfide battery	$2\ S_4^{2-} + 2e^- \rightarrow S_2^{2-}$	$Fe(CN)_6^{4-} \rightarrow Fe(CN)_6^{3-} + e^-$	[54]
Polysulfide/Iodide	$S_2^{2-} + 2e^- \rightarrow 2S^{2-}$ (Average oxidation states, actually consists of mixture of $S^{2-}/S_2^{2-}/S_3^{2-}/S_4^{2-}$)	$3I^- \rightarrow I_3^- + 2e^-$	[55]
Iron/Copper (See Chapter 2.5.2)	$Cu(NH_3)_4^{2+} + e^- \rightarrow Cu(NH_3)_2^+ + 2NH_3$	$Fe(CN)_6^{4-} \rightarrow Fe(CN)_6^{3-} + e^-$	[23]

From the redox couples in Table 4 pairs have to be created, which meet the requirements that were set in Chapter 2. Only redox species with a similar (positive or negative) charge and operating pH can be paired. A final cut was made in redox pairs:

- The hydration sphere theory from chapter 2.3.1 indicates that the Seebeck coefficients of the electrolytes in acidic conditions (Cr^{2+}/Cr^{3+}, Fe^{2+}/Fe^{3+}, V^{2+}/V^{3+}) are likely to be similar. This would not result into a sufficiently large driving force for the system.
- The same can be said for pairing the iron or cobalt based systems in the alkaline category of Table 4. Of all the iron and cobalt based electrolytes, $Fe(CN)_6^{3-}/Fe(CN)_6^{4-}$ is by far the most used and proven electrolyte and has experimental data on the Seebeck coefficient, it is therefore chosen as the electrolyte to use for pairing.
- The copper ammonia ($Cu(NH_3)_n$) electrolyte could not be paired with another, since it is the only positively charged redox specie. It cannot be separated from other redox couples by a monopolar ion exchange membrane.

The selected electrolytes are displayed in Table 5 below.

Table 5. The selected electrolytes for the TREC application. The half-cell potentials at room temperature (E_0) are reported versus the standard hydrogen electrode (SHE). The E_0 of polysulfide is marked red, because it falls outside of the water splitting window for the neutral conditions reported by Li *et al.* [55]. **A**: Estimated Seebeck coefficients. The values are questionable, since the coefficients in the paper do not agree with experimental data for Fe^{2+}/Fe^{3+}.

Redox couple	**α(mV/K)**	**Reference**	**E_0 (V vs SHE)**
Neutral			
$Fe(CN)_6^{4-} \leftrightarrow Fe(CN)_6^{3-} + e^-$	-1.4	[13]	0.436
$3I^- \leftrightarrow I_3^- + 2e^-$	-0.186[A]	[56]	0.535
$2S^{2-} \leftrightarrow S_2^{2-} + 2e^-$	-1.52[A]	[56]	-0.64
Alkaline (pH > 12)			
$Fe(CN)_6^{4-} \leftrightarrow Fe(CN)_6^{3-} + e^-$	-1.4	[13]	0.436
$ACA\text{-}2H \leftrightarrow ACA + 2e^- + 2H^+$	?	NA	-0.62

These electrolytes lead to two pairs:

1. The first choice is the pair of $Fe(CN)_6$ as catholyte and ACA as anolyte (electrolyte at anode/cathode) at alkaline conditions. Lin *et al*. [44] reported that this is a working and efficient RFB with long cycling stability. The Seebeck coefficient is unknown for ACA. It could be a positive Seebeck coefficient which would result in a large α for the full cell.

2. The second choice is the pair of I^-/I_3^- as catholyte and $Fe(CN)_6$ as anolyte at neutral conditions. The combination of these two electrolytes has not yet been reported in literature, so it is not yet proven that a RFB system like this could actually work. Both of the reported Seebeck coefficients are negative, which results only a moderately large α for the full cell.

4.1.3. Characterization of electrolytes

In this section the electrochemical characterization of the selected electrolytes is reported. The most key parameter here is the Seebeck coefficient of ACA/ACA-2H, since it determines the choice between the 2 pairs that were selected in the previous section.

Seebeck coefficient of $Fe(CN)_6^{3-}/Fe(CN)_6^{4-}$:

To test the setup, the Seebeck coefficient of the $Fe(CN)_6^{3-}/Fe(CN)_6^{4-}$ was measured. This is a commonly used redox couple, and the Seebeck coefficient of -1.4 mV/K was published in various articles [11, 13, 28].

The Seebeck coefficient was calculated by measuring the half-cell potential for 4 cycles of a CV scan at 8 different temperatures. A line was fit through these 32 points using the polyfit function of NumPy in Python. The slope of this line is the Seebeck coefficient. The CV scans and the fit are shown in Figure 16.

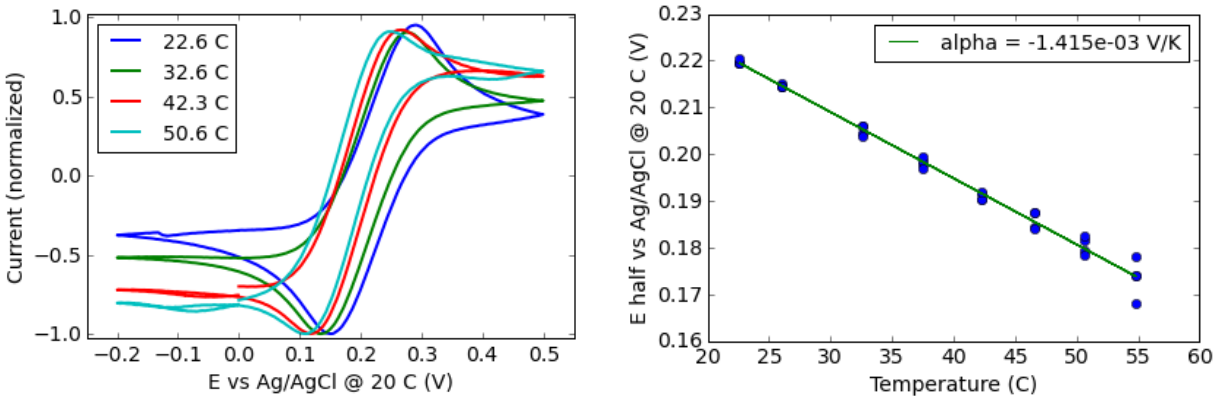

Figure 16. Electrochemical measurements of a solution of 0.1M $K_3Fe(CN)_6$, 0.1M $K_4Fe(CN)_6$ and 0.3M KCl (1 M K^+) **Left:** Four cycles of the CV scans at different temperatures, the currents are normalized on the absolute largest current. **Right:** Half-cell potential vs temperature, each blue dot represents the half-cell potential of one CV cycle. A linear fit was done through all the points to find the Seebeck coefficient, $R^2 = 0.989$

From Figure 16 the following can be concluded:

- The cyclic voltammograms are symmetric: the area of the negative current is equal to the positive current. The area in a CV scan corresponds to the amount of electrons transferred during the scan. Since the area of the negative current is equal to that of the positive current, the reaction goes equally fast in both directions. This means that the reaction is reversible.
- At room temperature the half-cell potential is +0.22 V vs Ag/AgCl. The Ag/AgCl has a potential of +0.22 V vs SHE. This means the half-cell potential is +0.44 V vs SHE, which agrees with literature values from Table 5.
- For higher temperatures the sharpness of the peaks decreases. The peak of a CV is caused by diffusion limitations and since diffusion is faster at higher temperatures the peaks are smaller relatively to the final current.
- The Seebeck coefficient was measured as -1.4 mV/K, which perfectly agrees with the literature. At higher temperatures, there is more noise in the measurement of the half-cell potential. This is caused by the reduced sharpness of the peaks described in the previous point, since the peak location is less defined.

From the points above it can be concluded that the built setup is capable of measuring the Seebeck coefficient and half-cell potentials accurately.

Seebeck coefficient of ACA/ACA-2H:

In order to measure the Seebeck coefficient of ACA, it had to be synthesized first (see Chapter 3.2). The synthesis is a simple one step reaction at room temperature from readily available reactants[36].

To check if a pure compound was synthesized, UV-VIS spectrometry and ^{1}H-NMR measurements were done and compared with the supplementary information of Lin et al[44]. From the ^{1}H-NMR (Appendix D) it can be concluded that pure ACA was indeed synthesized, but that not all the solvent (acetic acid) was washed off during the purification. In the UV-VIS spectra (Figure 17) a peak appears at 275 nm that is not observed in the graphs from Lin et al. Two reasons could be given for that:

- This peak is due to the acetic acid still present in the mixture. However acetic acid mostly absorbs around 220 nm[57], so this is unlikely.
- Lin et al used a polystyrene cuvette for their measurements. These cuvettes are only suggested for wavelengths larger than 340 nm[58], since polystyrene absorbs light at wavelengths lower than 300 nm. The noise observed in Figure 17 is likely due to the filtering of the absorption spectrometer.

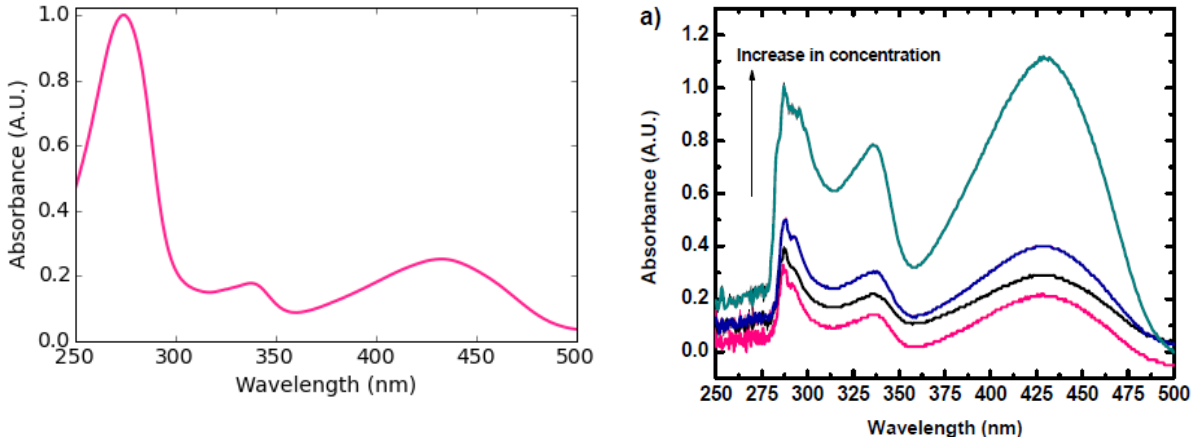

Figure 17. **Left:** UV-VIS measurement Absorption spectra were measured using a Perkin-Elmer Lamda 40 UV-VIS spectrophotometer at room temperature. The solutions were prepared in 10mm SUPRASIL Quartz Cuvettes from Helma Analytics by dissolving ACA in demineralized water. The concentration of ACA in the measurement was around 80 µM. **Right:** Data from literature [44], the pink line corresponds to the same concentration as the graph on the left.

For a CV-scan both the oxidized and reduced form need to be present. Therefore 20 mL of ACA electrolyte was reduced to a 50/50 mix of ACA and ACA-2H (more details on this in Chapter 3.1). The electrochemical measurements of ACA are shown in Figure 18 below.

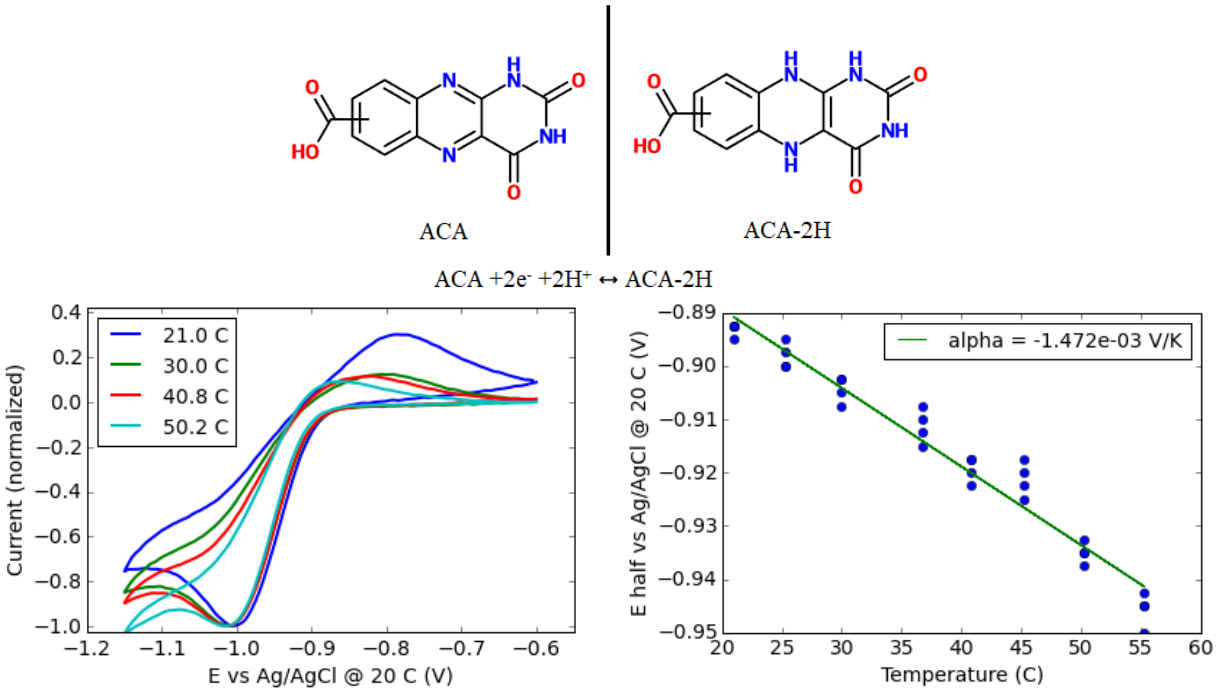

Figure 18. Electrochemical measurements of a solution of 0.025M ACA, 0.025 M ACA-2H, 0.1 M KOH and 0.9M KCl (1 M K^+) **Top:** Chemical structure of ACA and ACA-2H with the corresponding redox reaction. **Bottom left:** Four cycles of the CV scans at different temperatures, the currents are normalized on the negative peak. **Bottom Right:** Half-cell potential vs temperature, each blue dot represents the half-cell potential of one CV cycle. A linear fit was done through all the points to find the Seebeck coefficient, $R^2 = 0.956$

Figure 18 shows that the cyclic voltammograms are not symmetric. Lin *et al.* do however report that the redox reaction of ACA is reversible[44]. There are two other factors that could play a role in the asymmetry:

1. The asymmetric behavior occurs because 2 H^+ atoms have to be attached to and removed from the ACA molecule. This most likely happens in a different order, causing different reaction kinetics and therefore a different peak shape.
2. At the lower voltages the hydrogen evolution reaction starts causing a large negative current. The hydrogen evolution reaction has a Seebeck coefficient of +0.87 mV/K, which causes the reaction to start at higher voltages, explaining the bigger dip at -1.15 V at higher temperatures.

The asymmetry does cause an issue, since the formula for calculating the half-cell potential **(3)** only works for symmetric CV-scans. The temperature effect on the peeks is also asymmetric. Only the cathodic peaks undergo a change due to temperature. The anodic peak might be unchanged because the Seebeck effect of the hydrogen evolution and the ACA redox reaction have an opposite effect on the peak, causing it to remain unchanged. Equation **(3)** was used anyway, since it seemed the only way to calculate the Seebeck coefficient. By taking the average of the shift in the cathodic and anodic peak, a Seebeck coefficient of -1.5 mV/K was calculated.

A full cell of ACA and $Fe(CN)_6$ has an α of 0 – 0.1 mV/K, which is too low for any practical applications. The focus therefore shifted to the second choice, the pair of I^-/I_3^- and $Fe(CN)_6$.

Seebeck coefficient of I^-/I_3^-:

Since the value of the Seebeck coefficient was questionable for the I^-/I_3^- couple (see annotation in Table 5), it was decided to validate it by measurements. At the time of doing these measurements, only small amounts of iodine and potassium iodide were available. The measurements were therefore done at lower concentrations than for the full cell in section 4.2.2. Also a 1 I_2:10 KI ratio was used since I_2 dissolved very slowly (multiple days) at lower ratios. The electrochemical measurements of I^-/I_3^- are shown in Figure 19 below.

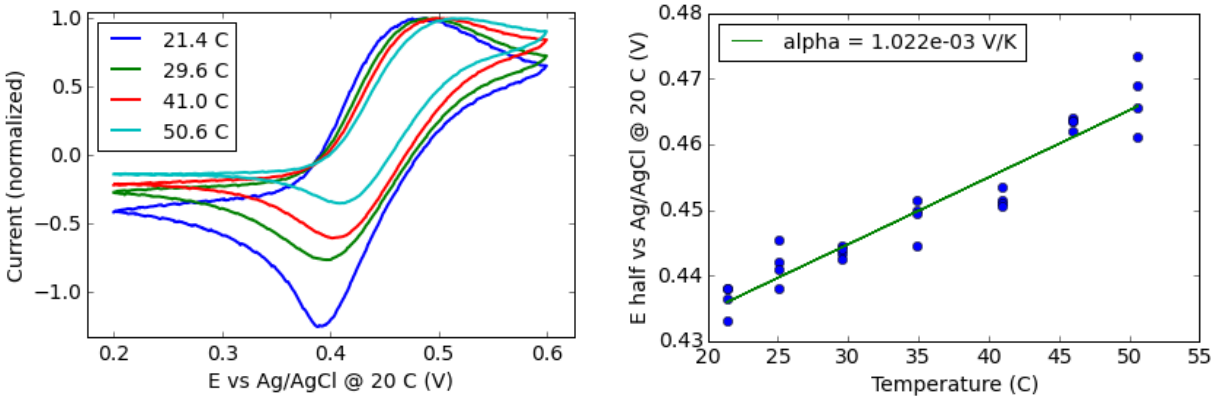

Figure 19. Electrochemical measurements of a solution of 0.01 M I^-, 0.001 M I_3^- and 1 M KCl (1 M K^+) **Left:** Four cycles of the CV scans at different temperatures, the currents are normalized on the maximum positive current. **Right:** Half-cell potential vs temperature, each blue dot represents the half-cell potential of one CV cycle. A linear fit was done through all the points to find the Seebeck coefficient, $R^2 = 0.911$

The CV-scans of Figure 19 figure show a different behavior than was seen before. At the start of the measurement the cyclic voltammogram is symmetric, indicating a reversible reaction. At higher temperatures, the magnitude of the anodic peak significantly decreased. During the experiment, the color of the mixture also changed (Figure 20) from dark orange to yellowish to eventually colorless. The color is caused by the I_3^- ion, which is a product of the following equilibrium reaction.

$$I^- + I_2 \rightleftharpoons I_3^-$$

From these two observations, it can be concluded that iodine evaporated from the mixture during the heating. A change in the I^- : I_3^- ratio also causes a change in diffusion limitations, explaining why the anodic peak size decreased in Figure 19. The half-cell potential (+0.66 V) at room temperature is higher than is displayed in Table 5, this is most likely the result of the nonstandard I_2:KI ratio.

The Seebeck coefficient (+1.0 mV/K) of the I^-/I_3^- couple, turned out to be positive, unlike it was predicted in Table 5. To check that it was indeed the Seebeck effect (and not the evaporation of Iodine) that caused this shift in half-cell potential, a second experiment was done. Here the electrolyte was heated, then cooled down again for a second measurement. If hysteresis occurs, the concentration difference would cause a change in potential.

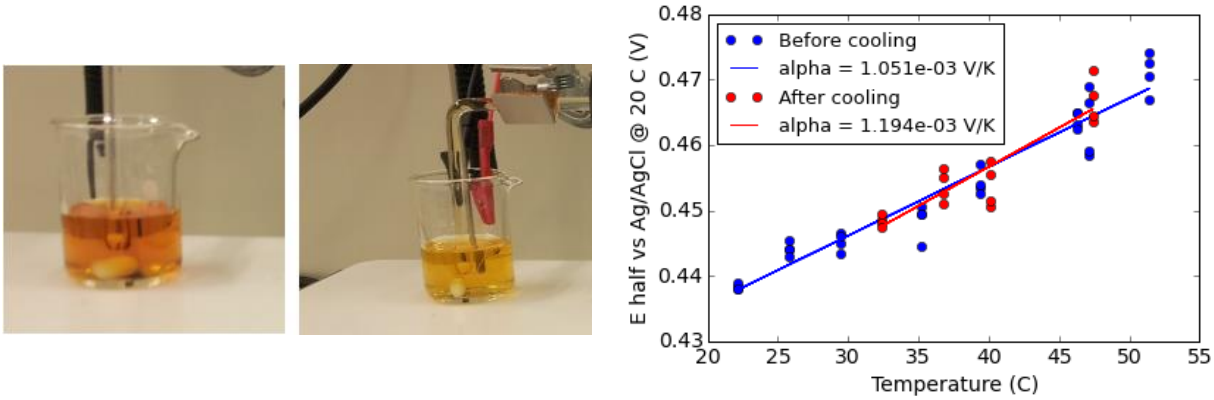

Figure 20. Investigation of the color change of I^-/I_3^- during heating. **Left:** Photo of the electrolyte before heating. **Middle:** Photo of the electrolyte after heating. **Right:** Potential vs temperature before and after cooling. Blue dots and lines are before cooling, red are after cooling. A linear fit was done through all the points to find the Seebeck coefficient for both datasets. R^2 before cooling = 0.932. R^2 after cooling = 0.829

From Figure 20 it can be concluded that the Seebeck coefficient is indeed +1.0 mV/K. A full cell consisting of $Fe(CN)_6$ and I/I_3 then meets all the requirements set in Chapter 2, with the only downside being that $K_4Fe(CN)_6$ is only moderately soluble (~0.6 M at maximum). For I/I_3 solutions of 2 M and higher have been reported[55].

In order to start experiments with a full cell, more potassium iodide and iodine were ordered. The experiments with the flow cell are discussed in section 4.2.

4.1.4. Effect of concentration and addition of ethanol

During the last two weeks before handing in the thesis, two bachelor students performed experiments to investigate the effect of concentration and the addition of ethanol on the Seebeck coefficient. Unfortunately there was not enough time to process all the data before handing in the reports however the overall trends that were observed are:

- The Seebeck coefficient of $Fe(CN)_6$ becomes stronger negative with higher wt% of ethanol in the mixture. The solutions of 0, 10 and 20 wt% showed in a decrease of -1.3 to -2.3 mV/K.
- The Seebeck coefficient of I/I_3 becomes stronger positive with higher wt% of ethanol in the mixture. The solutions of 0, 10, and 20 wt% showed in an increase of +0.9 to +1.9 mV/K.
- The Seebeck coefficient of I/I_3 increased for lower concentrations (numbers still need to be calculated but the change is in the order of 0.1-0.3 mV/K)
- The effect of the concentration of $Fe(CN)_6$ still has to be processed.

However, a problem was also observed: KCl does not dissolve in ethanol. This results into having smaller concentrations of conductive ions and thus a higher internal resistance. There most likely exists an optimum ethanol wt% where the losses due to resistance and gains due to the increased Seebeck balance each other out.

Addition of ethanol to the electrolytes will increase the full cell α for the $Fe(CN)_6$ and I/I_3 RFB system by almost a factor two. Also the Seebeck coefficient of I/I_3 in 4.2 might turn out to be lower for the full cell, since higher concentrations will be used.

4.2. Designing and operating of the full system

As was already mentioned in chapter 1 and 2, a TREC system will be designed based on flow batteries. The setup of the flow cell will briefly be discussed in 4.2.1. The results of the experiments with the flow cells will be presented and discussed in 4.2.2.

4.2.1. Design of the flow cell

The crucial part of this system is the flow cell, in which the redox reactions take place. The flow cell design was based on a redox crossflow cell previously designed by David Vermaas [38]. This design has an electrode with a circular radius of 1 cm. As is mentioned in Appendix A, energy losses scale with current density and the power increases with a larger current. The current can also be increased by making the electrode area larger, while keeping the current density constant. To improve the efficiency of the TREC, the electrode radius was therefore scaled up to 5 cm. This resulted into a 25 times larger area. A larger current results in a bigger conversion of the chemicals, which results in a temperature change. By having bigger currents this temperature change should be easier to measure. Apart from giving a larger current, this flow cell is much easier to assemble and disassemble.

A schematic representation of the flow cell setup is shown in Figure 21.

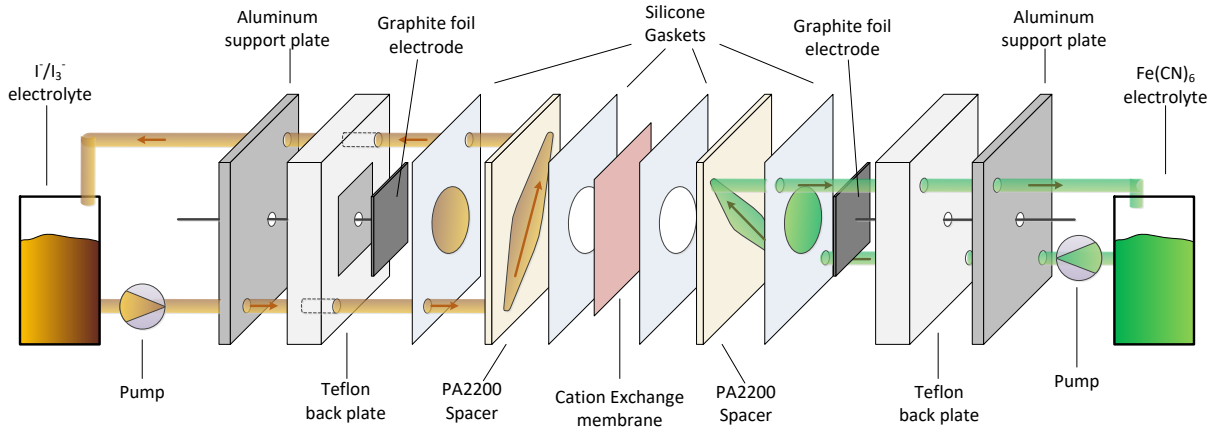

Figure 21. Schematic diagram of the crossflow flow cell setup. The two electrolyte solutions flow in from the bottom. In the middle of the cell there is a circular gap with radius of 5 cm on two sides where the electrolyte makes contact with the electrode and the membrane. It then flows out on the top, where it goes back to the beaker. The potential difference can be measured between the two graphite foil electrodes.

The next section will discuss the experiments with the flow cell.

4.2.2. Experiments with the flow cell

Based on the electrochemical data from section 4.1.3, the Seebeck coefficient and open cell potential should be +2.4-2.5 mV/K and ~0.1 V respectively for the chosen redox couples.

A first run was performed at room temperature (21 ºC) to test basic operation. The potential was measured for 17 different currents: The cell was run for some time on open cell (zero current). Then at -80 mA until a steady condition was reached, followed by +80 mA, -70 mA, +70 mA, etc. until an open cell condition was reached again. The results of this experiment are shown in Figure 22 below.

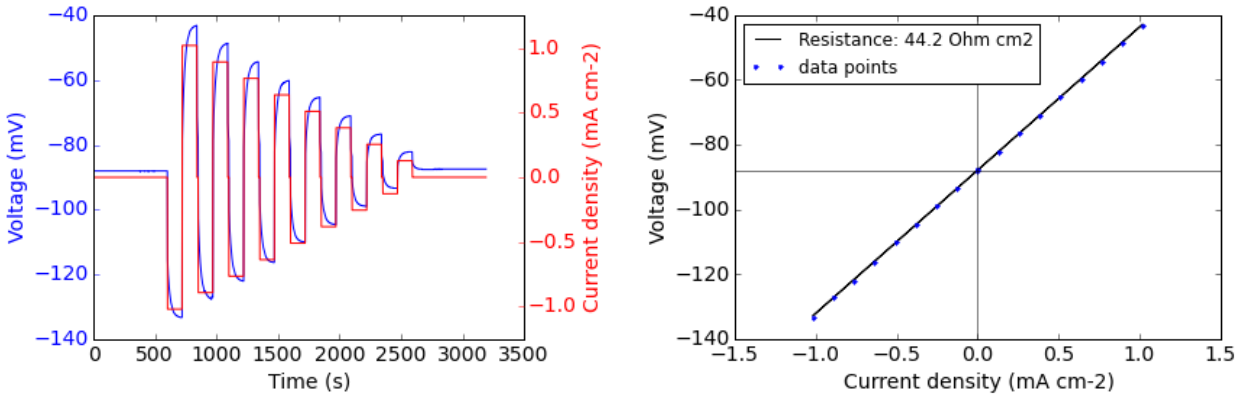

Figure 22. **Left:** Stepwise I/V plot versus time of the flow cell at room temperature (21 ºC). **Right:** The settled potentials at the end of every step, plotted against the current. A linear fit was done to find the Ohmic resistance of the flow cell. $R^2 = 1.000$

It can be assumed that the process is reversible, since the open cell potential does not change (±0.5 mV) after running the cell for almost an hour. A fit of the I/V curve resulted in a high resistance of 44.2 Ω cm^2, this is an order of magnitude larger than for other flow batteries from literature: The ACA-$Fe(CN)_6$ RFB[44] had a resistance of 1.03 Ω cm^2 and the polysulfide/iodide [55] had a resistance of 3-4 Ω cm^2. These two systems here have the same redox couples as in our battery and only slightly higher concentrations, both RFBs employed porous carbon electrodes.

Since the electrode material and redox couples are the same for the literature and the experiments of this thesis, it can be concluded that the high resistance is likely due to the design of the cell. The compartments are much thicker than the cells from literature (~5 mm compared to less than 1 mm), which causes a strong resistance due to the diffusion of K^+ ions across a larger distance. Also more than 50% of the membrane area is covered by the porous disk (Figure 12) which makes it even more difficult for the K^+ ions to be transported. A better cell design and porous electrodes might reduce the resistance by a factor 5 to 10.

After this first test run the cell was disassembled (Figure 23), to see if the electrode and membrane were still intact. The graphite foil electrode and membrane were undamaged. The silicone gaskets changed in color (could not be washed of) and also changed in shape. In the middle photo of Figure 23 a strong leakage of the iodide side (brown) to the hexacyanoferrate (green) side was observed. It seems that the membrane prevented the iodide electrolyte from spreading into the other electrolyte flow compartment, as this remained mostly uncolored.

After reassembling the cell, it was observed that the two sides were no longer separated, as fluid from one side could flow into the other. Further experiments were done with new silicone gaskets. No data is available on the iodine resistance of silicone[59], but after these experiments it is clear that silicone is not very resistant.

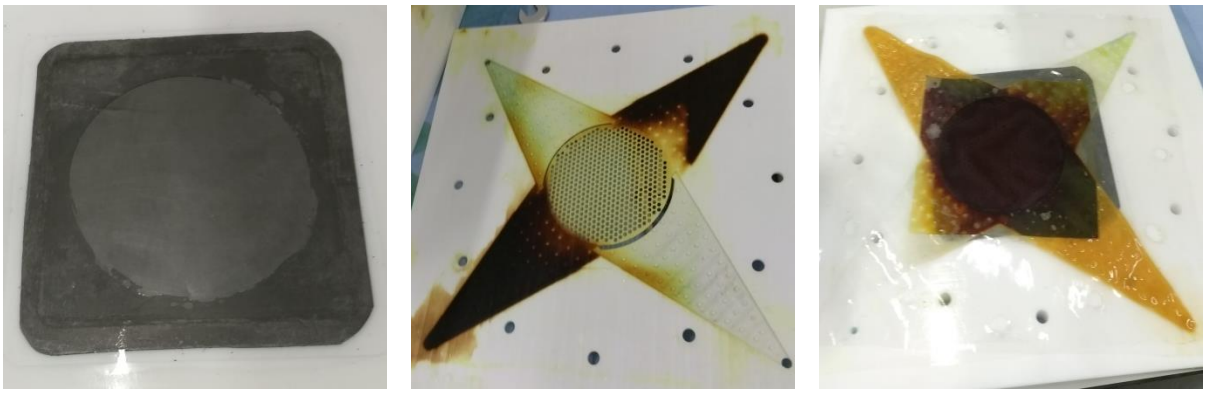

Figure 23. Photos of the status of the flow cell after the first run. **Left:** The carbon electrode with gasket on top **Middle:** Spacer from the hexacyanoferrate side. **Right:** Strongly colored silicone gasket (normally transparent) and membrane in the center (normally light yellowish). The membrane was cut in a square shape of which the edges can still be seen through the gasket.

For the second experiment, the cell was connected to a heat bath and the in- and outflow temperatures were measured. Four measurements were done, with the heating bath at 30, 35, 40 and 45 ºC. During the 45 ºC measurement another leakage occurred and the experiment had to be stopped (see Figure 24). The open cell voltage was clearly affected, and therefore it was decided to exclude the data from 45 ºC from the calculation of the Seebeck coefficient.

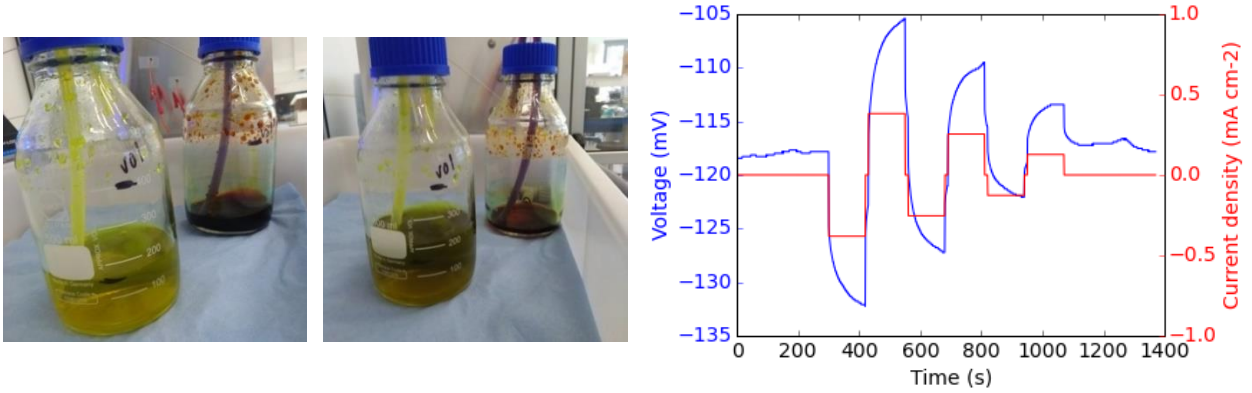

Figure 24. Flow cell experiment with heat bath at 45 ºC. **Left:** Photo of electrolytes before the experiment. **Middle:** Photo of the electrolytes after the experiments. It can be seen that the color of the hexacyanoferrate (green) became much darker, and the flask of the Iodine (dark brown) almost empty. **Right:** I/V measurement. There is noise present in this I/V curve, also the open cell potential at the beginning and end are not the same.

Throughout each measurement, the temperatures remained constant (±0.1 C). The temperature at the electrode is of interest for the Seebeck coefficient. This temperature was assumed to be the average of the in- and outflows. The temperatures and Seebeck coefficient are shown in Figure 25 below.

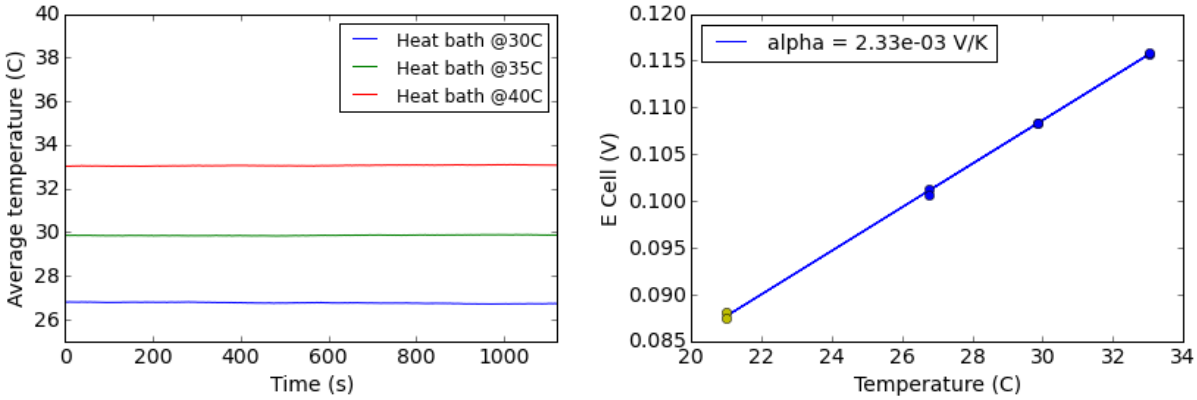

Figure 25. **Left**: Average temperatures during the measurement for different heat bath temperatures. The temperatures were averaged over the two inflow and two outflow streams. **Right:** Open cell potential vs the temperature. A line is fitted to find the Seebeck coefficient. The yellow dots are the open cell potential at room temperature (the lab temperature is 21 degrees) reported at the beginning of this chapter. $R^2 = 0.999$

The Seebeck coefficient is slightly lower than, but very close to the expected +2.35-2.45 mV/K. This could be because of the higher concentrations of I^- and I_3^- compared to the measurements of Figure 19. The full cell potential at room temperature is a bit lower than predicted, which could be due to a different I/I_3 ratio in the flow cell electrolyte compared to the CV measurements of 4.1.3. A Seebeck coefficient of +2.33 mV/K is very high. For aqueous thermogalvanic cells, there is only one article[28] which reports a higher Seebeck coefficient: -2.9 mV/K for hexacyanoferrate in water-organic mixtures.

The Ohmic resistances of the flow cell were measured as well during the experiment (see Figure 26). The resistance decreases strongly with temperature, which is logical since reaction kinetics increase and diffusion limitations decrease with higher temperature. The setup allowed to measure at four temperatures only. While these are insufficient data points to draw strong conclusions, some fitting of the data will be done anyway.

The resistances appear to be on a straight line, and show a good fit with linear regression. However in electrolytes the resistance should be a hyperbolic function of the temperature[60]:

$$R(T) = \frac{R_0}{\left(1 + \theta(T - T_0)\right)} \qquad \textbf{(18)}$$

R_0 is the resistance at a reference temperature T_0 (chosen to be 30 ºC), θ is a temperature coefficient (of units $ºC^{-1}$) and T is the temperature in ºC. The fit of this function and θ are also shown in Figure 26. Fitting a hyperbolic function through four points is inaccurate, but it is necessary to have a this function for resistance at higher temperatures for the model discussed in the next section. A line would have resulted in negative resistances at temperatures above 82 ºC, which is unphysical.

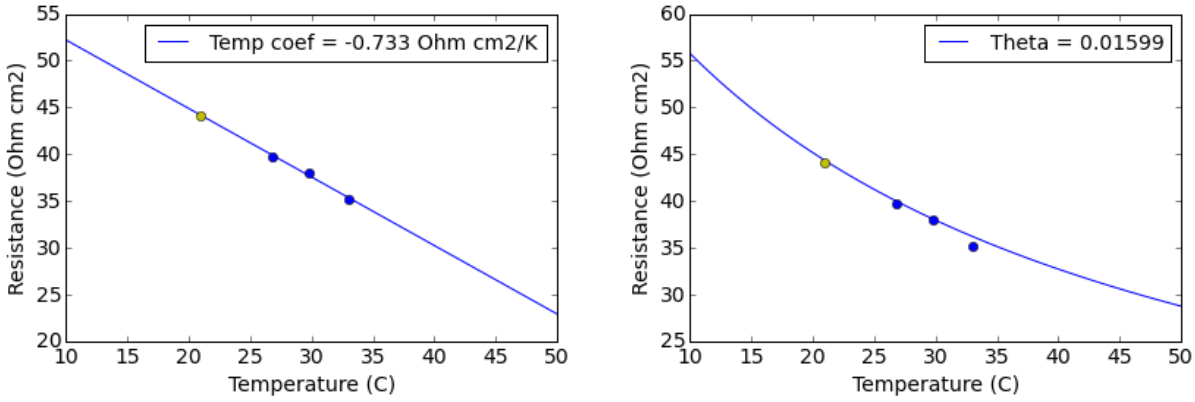

Figure 26. Fits of the Ohmic resistance of the full cell. **Left:** Linear fit, in the legend the slope of the line is displayed. $R^2 = 0.997$ **Right:** Hyperbolic fit using **(18)**, Theta is temperature coefficient θ. $R^2 = 0.873$

Another measurement at room temperature with new electrolytes resulted again in leakage. It was concluded that the flow cell was too damaged for more experiments. The limiting factor of the design seems to be the silicone gaskets, which are not resistant enough to iodine.

4.3. A numerical approach of the system

In this section ASPEN Plus will be used to model the design in order to give an estimate of the heat to power efficiency, since the damaged gaskets prevented measuring it experimentally. ASPEN Plus was chosen as modeling tool, since the thermal properties of water are well defined and all the properties of a heat exchanger can be calculated.

The potential of a flow cell can be estimated with the following formula:

$$V(T) = E_0 + \alpha(T - T_0) \pm I_{dens}R(T) - \frac{RT}{nF}\ln\left(\frac{[I^-]^3[Fe(CN)_6^{-3}]^2}{[I_3^-][Fe(CN)_6^{-4}]^2}\right) \quad \textbf{(19)}$$

E_0 is the potential at T_0, the Seebeck coefficient (α) is +2.33 mV/K as was shown before, I_{dens} is the current density and the R(T) is the Ohmic resistance, which is modeled by **(18)**. The last term is the contribution of the concentration difference from the Nernst equation. However, the TU Delft desktop version of ASPEN Plus crashes whenever a logarithm is calculated. It was decided to simplify **(19)** to:

$$V(T) = E_0 + \alpha(T - T_0) \pm I_{dens}R(T) \quad \textbf{(20)}$$

It can be simplified, because the effects of the last term on the potential losses are minimal at low currents, compared to the Ohmic losses, as displayed in Figure 27 below.

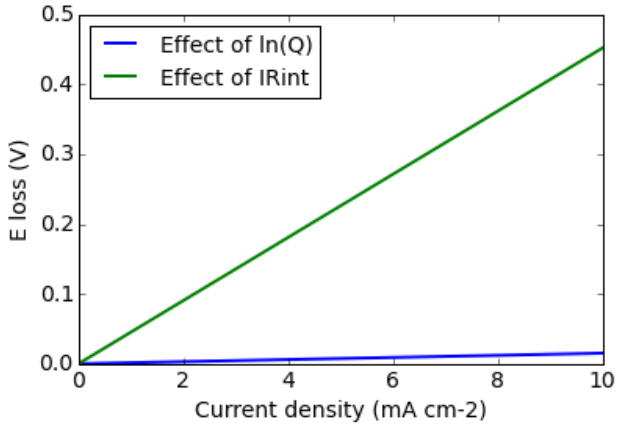

Figure 27. Potential losses at different current densities of two different effects. The green line represents the Ohmic losses, the blue line the last term of equation **(19)**. The effect of the blue line scales with the conversion in the flow cell, so if a larger area is take, the effect will be larger.

The setup is simulated by 2 reactors, a heater, a cooler and a heat exchanger. The electrolytes are modeled as water, since the heat capacity of the mixture is similar to that of water. The electrochemistry and reaction heat are added through calculator blocks. For a more detailed description of the model, see Chapter 3.5.

First a base case simulation was done to find the optimum current density to run at based on the maximum power (the first two are values used during experiments):

- Flow rate: 1 mL/s
- Electrode area: 78.54 cm^2
- T_{hot}: 90 ºC
- T_{cold}: 20 ºC
- Heat exchanger approach (hot inlet- cold outlet temperature difference): 1 ºC

The optimal current density is 1.27 mA/cm^2 (see Figure 28). This is quite low because of the low open cell potential and high internal resistance. The latter could be reduced with higher salt concentrations and a thinner flow region.

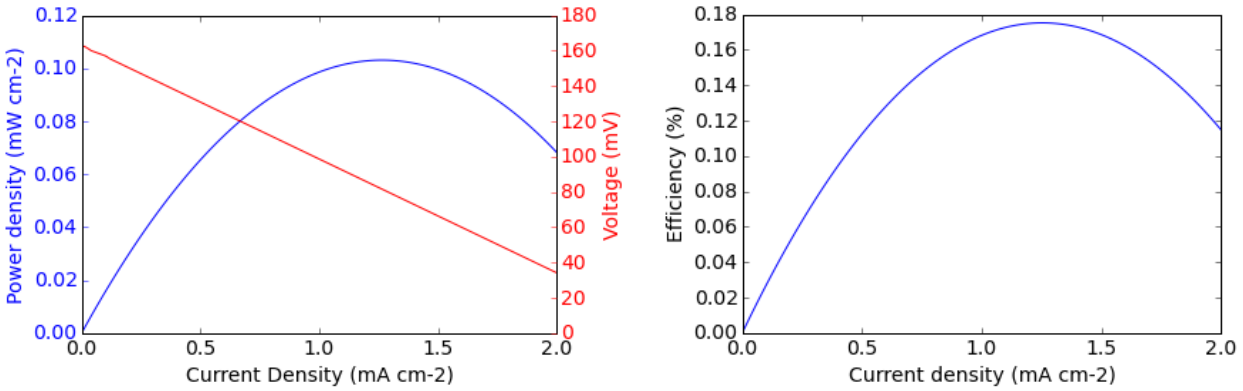

Figure 28. The effects of current density on the design simulated with ASPEN Plus. **Left:** Sensitivity analysis of the current density vs the system power and voltage. The maximum power is 8.10 mW at 1.27 mA/cm^2. **Right:** Current density vs heat to power efficiency. The maximum efficiency is 0.175% at 1.25 mA/cm^2.

The maximum power for our design is only 8.10 mW. Too give a comparison: the pump that was used for this cell uses 75 W, resulting in the system only consuming energy instead of producing from waste heat. However the model allows us to simulate the TREC system beyond the current design, assuming the Seebeck coefficient and equation for the resistance scale well. Two parameters can still be changed:

- The conversion of flow cell (either by increasing the electrode area or reducing the flowrate)
- The effectiveness of the heat exchanger.

Increasing the area of the electrode increases both the power and heat to power efficiency of the system (Figure 29). It is important to note that the accuracy of the model also decreases for higher electrode area, since the contribution of the ln(Q) term (Figure 27) becomes larger. This causes an overestimation of the power and efficiency.

With electrode area of 1 m^2 an efficiency of 6.8% is even predicted, this is already 35% of the Carnot efficiency! An electrode area of 1 m^2 is reachable by scaling up the system, or by creating cell stacks (multiple cells in series). However, even for a 1 m^2 electrode the electrical power is only 1 Watt, which is most likely not enough to pump the electrolytes through the cell.

The efficiency is also strongly affected by the heat exchanger efficiency (see Figure 29). The very steep curve indicates that a large amount thermal energy is lost in heating the system. From the heat exchanger properties in ASPEN, it can be seen that a countercurrent heat exchanger, for a temperature approach of 0.1 ºC requires a heat exchange area of 3.6 m^2. For 1 ºC it would require only 0.33 m^2.

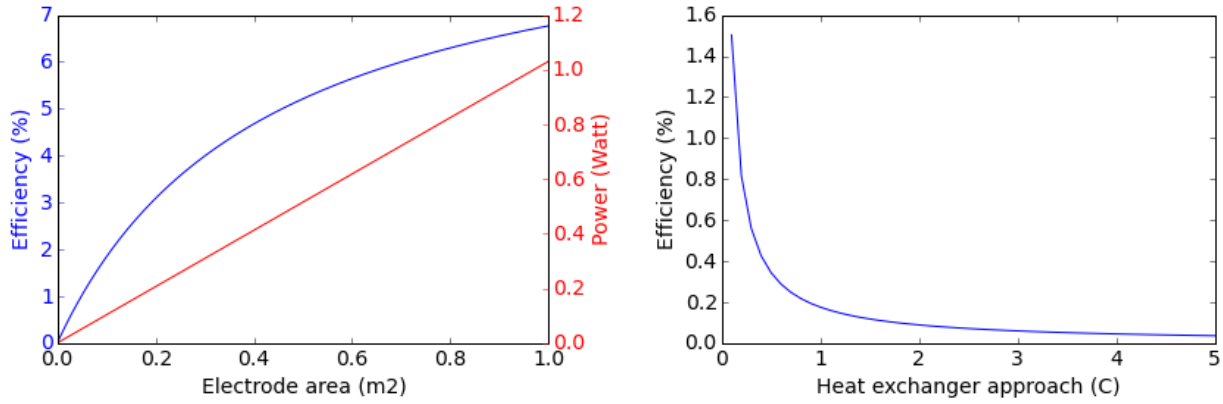

Figure 29. Analysis of heat exchanger approach and Electrode area on the effectiveness of the design, simulated with ASPEN Plus. **Left:** Effect of the electrode area on the efficiency and power, the temperature approach is 1 ºC here. **Right**: Effect of the heat exchanger approach (hot inlet- cold outlet temperature difference) on the efficiency. The electrode area is 78,5 cm^2 here.

Using an online tool [61], the pressure drops were calculated for a straight tube of 6 mm inner diameter, this is what we used for tubing during experiments. A heat exchanger with an area of 3.6 m^2 results in a pressure drop of 120 mbar, a heat exchanger with an area of 0.33 m^2 in a pressure drop of 11 mbar. This pressure drop needs to be multiplied by two, since both a hot and cold stream go through the heat exchanger. After the heat exchanger the stream flow past the heat source and sink to reach the final temperatures. This is only a small temperature increase. It is assumed that this is only 20% of the pressure drop resulting from a 1 ºC heat exchange approach. The pressure drop due to the heating and cooling then becomes:

- 0.1 ºC approach: 245 mbar
- 1 ºC approach: 27 mbar

The pressure drop in the flow cell will be estimated by looking at the electrode area, which will be calculated by the relation for a pressure drop between 2 plates. For the ease of calculation, it is assumed that the electrode has a square shape. The theoretical pressure drop for laminar flow between two plates is defined as follows[62]:

$$\Delta p = \frac{12\mu \cdot L \cdot Q}{d^3 \cdot w} \quad \textbf{(21)}$$

Here Δp is the pressure drop in Pa, μ the dynamic viscosity in Pa·s, L the length of the electrode in m, d the distance between the two plates in m, w the width of the electrode in m and Q the flow rate in m^3/s. For a square electrode this simplifies to:

$$\Delta p = \frac{12\mu \cdot Q}{d^3} \quad \textbf{(22)}$$

Using the parameters of this cell, d = 2 mm, Q = 1 mL/s, μ = 1.002 10^{-3} Pa·s at 20 ºC or 0.315 10^{-3} Pa·s at 90 ºC. Both electrolytes go through a flow cell at 20 and 90 ºC. The total pressure drops because of the flow cells then is 4 Pa, which is negligible compared to the heat exchanger.

The required pump power can then be calculated with:

$$P_{pump} = \frac{\Delta p \cdot Q}{\eta_{pump}} \quad \textbf{(23)}$$

Here P_{pump} is the pump power in Watts and η_{pump} the pump efficiency. For a small scale system like this a magnetic drive pump could be used, which have an efficiency of up to 70%[63]. In order to not underestimate the pump power consumption, it will be assumed that the pump efficiency is 50%. A heat exchange approach of 1 ºC requires a pressure drop of around 0.05 bar including all parts, which corresponds to a pump power of 5 mW. This means that the un-optimized flow cell of this thesis could theoretically produce electricity from waste heat.

Making a thinner flow cell could reduce the resistances significantly, however the pressure drop over the cell will also increase cubically according to equation **(22)**. For reverse electro dialysis, an optimum thickness was found to be in the order of 0.2 – 0.5 mm thick, which more than 10 times smaller than our current flow cell[64]. The design could be improved significantly.

The model could be improved by addition of the ln(Q) term, whether that be through using different software, or by fixing the problems of ASPEN Plus. Measurements of the resistances at higher temperatures would also improve the accuracy of the R(T) function, and therefore the model. Finally a good estimation of the pressure drop and pump losses should be included into the efficiency calculation of the model, to give a good indication of the real heat to power efficiency.

5. Conclusion

In this thesis a flow battery system with iodine/iodide and hexacyanoferrate based electrolytes was designed to convert heat into power using the thermally regenerative electrochemical cycle (TREC).

A literature study was done in which many different RFBs were evaluated. From these systems, the most suitable electrolyte pair was:

- $Fe(CN)_6^{4-}$/ $Fe(CN)_6^{3-}$
- I^-/I_3

This is because these two have high and opposite Seebeck coefficients, no undesirable side reactions and are separable by an anion exchange membrane. The chemicals of these electrolytes also have moderately high solubility. The Seebeck coefficient of these electrolytes could be increased even further by the addition of ethanol.

In order to have net gain, the system needs to be running at a wide temperature interval (> 50 ºC) and with a low current density with the highest possible concentrations to reduce the internal resistance as much as possible.

The main causes for heat to power efficiency losses are:

- The Ohmic losses due to the internal resistance
- The heat required to heat the electrolyte to the hot operating temperature

Of these two the Ohmic resistance seems to have the biggest effect on the losses. This is because the potential difference between the cells is in the order of 100 mV which is easily overshadowed by the Ohmic loss. The cell design is the main cause for the high resistance, and making the cell thinner would reduce the resistance significantly.

We were not able to determine the efficiencies experimentally. The Iodine electrolyte damaged the cell's silicone gaskets, which resulted into mixing of the two electrolytes of the cell. This affected the potential so strongly that it was impossible to do sufficient reliable experiments.

From a simulation in ASPEN Plus it was concluded that the heat to power efficiency of such a system is heavily dependent on the electrode area and heat exchanger efficiency, but could eventually reach more than 50% of the Carnot efficiency for large electrode area (in the order of 1 m^2) and a heat exchanger approach of 0.1 ºC.

Finally, based on the current data it cannot be said whether the TREC based on flow batteries can compete with other low grade heat to power technologies. The design requires the pumping of electrolytes, which even for an optimized system most likely costs a large chunk of the energy that the TREC recovers. The system needs to be optimized and investigated further, before anything can be concluded about the potential of this technology.

6. Recommendations

The main drawback of the TREC based on flow batteries is the power required to pump the electrolytes through the system. To increase the power output it is recommended to do the following 3 changes:

- Increase the area of the electrode
- Reduce the internal resistance
- Increase the voltage difference

The first point speaks for itself. It requires either a bigger setup or several stacks of the cell. The second point can be solved by using higher concentrations of active species and KCl and a thinner cell, which results in less diffusion limitation. A different type of electrode might also reduce the resistance by improving the redox kinetics.

The last point can only be achieved with a bigger temperature difference or a redox pair with a higher Seebeck coefficient. The effect of added organic solvents should be investigated further, to find an optimum weight percentage for increasing the voltage difference.

For aqueous systems the options of anorganic redox electrolytes are limited due to side reactions and low solubilities, the $Fe(CN)_6$ and I^-/I_3^- are likely the best option. For higher Seebeck coefficients organic redox molecules or other types of solvents, e.g.ionic liquids or deep eutectic solvents, should be investigated.

It is important to improve the model (e.g. by measuring the resistance at higher temperatures). Therefore it is advised to continue the measurements at higher temperatures as well. If another student would continue to measure the efficiency of the current setup, the Silicone gaskets need to be replaced by another material. As of now, new FKM gaskets have been ordered, which should be resistant to all the used electrolytes[59].

The data from the two bachelor students still contains a lot of noise, and only a small amount of data points. It would be wise to continue the experiments and also see if the results can be replicated. This also gives a better indication of what the trends for different concentration and addition of organic solvents really is.

Also the pressure drop of the current system is simplified a lot. A CFD simulation of the system could give a better estimate of the pumping power.

Appendix A: Derivation of maximum power

The voltage (V) is split up in 3 parts:

- The open cell voltage (E_{OC}), this is the voltage when the current is 0
- The voltage drop due to Ohmic losses: IR_{int}
- The voltage losses (E_{loss}). Usually in the form of an overpotential: some reactions require a set extra voltage in order to occur. The overpotential is a loss of energy that usually cannot be avoided easily, unless choosing for a different reaction or electrode.

For a discharging battery, the voltage then becomes:

$$V = E_{OC} - IR_{int} - E_{loss}$$

The power of a battery per unit area with is then defined as:

$$P = V * I = (E_{OC} - IR_{int} - E_{loss}) * I = IE_{OC} - I^2R_{int} - IE_{loss}$$

Here P is the power, V is the cell voltage (after losses), I the current density and R_{int} the internal resistance.

The maximum power is found differentiating the power to the current density, and setting this to 0.

$$\frac{dP}{dI} = E_{OC} - 2IR_{int} - E_{loss} = 0 \rightarrow I = \frac{E_{OC} - E_{loss}}{2R_{int}}$$

The maximum power then becomes:

$$P_{max} = \frac{(E_{OC} - E_{loss})^2}{4R_{int}}$$

The total power can be increased by increasing the area of the electrode, since this does not affect the relative magnitude of the Ohmic losses.

Appendix B: Database of flow batteries

Color Legend

Acidic	Alkaline	Neutral	Organic solvents	Forms solids	Unfeasible	Other

Name		Anode reaction	Cathode reaction	Overpotential (V) for I = 0	Temperature range (°C)*	Additional information	Reference
Iron-Chromium		$Cr^{3+} + e^- \rightarrow Cr^{2+}$	$Fe^{2+} \rightarrow Fe^{3+} + e^-$	NA	*25-65*	Cross contamination	[19] [47] [48]
Iron-titanium		$Ti^{4+} + e^- \rightarrow Ti^{3+}$	$Fe^{2+} \rightarrow Fe^{3+} + e^-$	Yes, for Ti-reaction	*25-55*	Cross contamination	[46]
All-vanadium	Normal	$V^{3+} + e^- \rightarrow V^{2+}$	$VO^{2+} + H_2O \rightarrow VO_2^+ + 2H^+ + e^-$	0 V	10 - 40	Established technology[16]	[65] [66] [67]
	Added stabilizers				-20 – 50 [42, 43]		
Vanadium-Bromine		$2Br^- + Cl^- \rightarrow ClBr_2 + 2e^-$	$2VBr_3 + 2e^- \rightarrow 2VBr_2 + 2Br^-$	0 V	*10-40*	Stability of membrane in halide mixture unknown, also lifetime due cross-contamination unknown. Bromine gasses can form at 40 °C. [17]	[68]
Manganese-vanadium		$V^{3+} + e^- \rightarrow V^{2+}$	$Mn^{2+} \rightarrow Mn^{3+} + e^-$	0 V	*RT*	No real proof of concept, lifetime or temperature data	[69]
Vanadium-Iron	Chloride acid stabilizer	$V^{3+} + e^- \rightarrow V^{2+}$	$Fe^{2+} \rightarrow Fe^{3+} + e^-$	0 V	0-50	Charge capacity lowers after 50 cycles	[49]
	Mixed-Acid Supporting Electrolyte			0 V	0-50	Stable after 50 cycles at RT	[50]
Vanadium-cerium		$V^{3+} + e^- \rightarrow V^{2+}$	$Ce^{3+} \rightarrow Ce^{4+} + e^-$	Smaller than 0.15V (probably 0 V)	*25-60*	Low solubility of cerium salts	[70] [71]

Vanadium Polyhalide	$BrCl_2^- + 2e^- \rightarrow Br^- + 2Cl^-$ or $ClBr_2^- + 2e^- \rightarrow 2Br^- + Cl^-$	$VCl_2 + Cl^- \rightarrow VCl_3 + e^-$	0 V	5-40	Stability of membrane in halide mixture unknown, also lifetime due cross-contamination unknown. Bromine gasses can form at 40 °C. [17]	[68]
Tiron-Pb (Tiron is a benzene ring with SO_3 ,O and OH side-groups)	$PbSO_4 + 2e^- \rightarrow Pb + SO_4^{2-}$	$Tiron(OH)_2 \rightarrow Tiron(O)_2 + 2H^+ + 2e^-$	Smaller than 0.02 V (probably 0 V)	*RT*	pH < 4 needed for Tiron couple. Fast kinetics, needs activation for RFB.	[72]
Vanadium-glyoxal(O_2)	$V^{3+} + e^- \rightarrow V^{2+}$	$[OC]_{RED} + H_2O \rightarrow [OC]_{OX} + 2H^+ + 2e^-$	Oxygen polarization		Oxygen polarization at electrode, vanadium crossover	[73]
Vanadium cysteine	$V^{3+} + e^- \rightarrow V^{2+}$	$RSSR + 5\ Br_2 + 6\ H_2O \rightarrow 2\ RSO_3H + 10HBr$ And $10Br^- \rightarrow 5\ Br_2 + 10e^-$	0.4 V		Too complex, not efficient, small overpotential	[74]
Hydrogen Bromide RFB	$Br_2 + 2e^- \rightarrow 2Br^-$	$H_2 \rightarrow 2H^+ + 2e^-$	0.1V – 1 M Br_2 ~0.05 V – 2 M Br_2 0 V – 3 M Br_2	?-58.8 ºC Due to Br_2 boiling (at 1 atm pressure)	Simple kinetics, all over-potential from membrane. Br_2 boiling point in T range?	[75]
Metal-free organic redox molecules: 9,10-anthraquinone-2,7-disulfonic acid (AQDS)	$AQDS + 2e^- + 2H^+ \rightarrow DHAQDS$	$2\ HBr \rightarrow Br_2 + 2e^- + 2H^+$	0.1 V due to (de)protonation of AQDS	*RT*	1 M concentrations. Potential could be optimized with functional groups.	[76]
Titanium Manganese	$TiO^{2+} + 2H^+ + e^- \rightarrow Ti^{3+} + H_2O$	$Mn^{2+} \rightarrow Mn^{3+} + e^-$	NA	NA	Problems with Mn^{3+} stability, membrane crossover ($2Mn^{3+} + 2H_2O \rightarrow Mn^{2+} + MnO_2 + 4\ H^+$)	[77]
Bromine-polysulfide	$(x\text{-}1)Na_2S_x + 2e^- \rightarrow xNa_2S_{x-1}$ (x:2 or 4)	$2Br^- \rightarrow Br_2 + 2e^-$	0 V	?	Crossover	[78]

Vitamin B2 based	ACA + $2e^-$ + $2H^+$ → ACA-H_2 (ACA = Alloxazine Carboxylic Acid)	$Fe(CN)_6^{4-}$ → $Fe(CN)_6^{3-}$ + e^-	0 V	*RT*	Low energy efficiency 63-74%	[44]
All-Soluble All-Iron Aqueous Redox-Flow Battery	$[Fe(TEOA)OH]^-$ + e^- → $[Fe(TEOA)OH]^{2-}$ TEOA = Tri-ethanolamine	$Fe(CN)_6^{4-}$ → $Fe(CN)_6^{3-}$ + e^-	0	NA	Charge efficiency loss due to crossover of TEOA, large internal resistance (TEOA contaminates Nafion membrane, higher transfer resistance?)	[51] [52]
Alkaline flow battery based on the coordination chemistry of Fe and Co	$[Fe(TEOA)OH]^-$ + e^- → $[Fe(TEOA)OH]^{2-}$ TEOA = Tri-ethanolamine	$[Co(mTEOA)H_2O]^-$ → $[Co(mTEOA)H_2O]$ + e^- mTEOA = methyl-Tri-ethanolamine	Low voltage efficiency, but most likely 0	*RT*	Cobalt couple is not perfectly reversible. 5 M NaOH. Large Fe/Co ratio needed to prevent large loss of capacity.	[52] [53]
Iron/Copper	$Cu(NH_3)_4^{2+}$ + e^- → $Cu(NH_3)_2^+$ + $2NH_3$	$Fe(CN)_6^{4-}$ → $Fe(CN)_6^{3-}$ + e^-	NA	0-100	Uses both positive and negative redox ions, which are difficult to separate	[23]
All-chromium	Cr(III)-EDTA + e^- → Cr(II)-EDTA	Cr(III)-EDTA → Cr(V)-EDTA + $2e^-$	NA	NA	Sluggish reaction kinetics, very low efficiencies (8% in battery setup)	[79]
Aqueous polymer based	$Viologen^{2+}$ + e^- → $Viologen^+$	TEMPO → $TEMPO^+$ + e^-	0 V	*RT*	Energy losses from pumping due to high viscosity?	[80]
Ferro/ferricyanide polysulfide battery	2 S_4^{2-} + $2e^-$ → S_2^{2-}	$Fe(CN)_6^{4-}$ → $Fe(CN)_6^{3-}$ + e^-	0 V	*RT*	Cheap materials. However: Crossover problems at high temperatures, sluggish electrode reactions	[54]

Polysulfide/Iodide	$S_2^{2-} + 2e^- \rightarrow 2S^{2-}$ (Average oxidation states, actually consists of mixture of $S^{2-}/S_2^{2-}/S_3^{2-}/S_4^{2-}$)	$3I^- \rightarrow I_3^- + 2e^-$	0 V	*RT*	High cycling stability, High solubility (<6.0M) *Crossover problems at high temperatures?*	[55]
Total Organic aqueous with Methyl Viologen and 4-HO-TEMPO	$MV^{2+} + e^- \rightarrow MV^+$	4-OH-TEMPO $\rightarrow$ $[4\text{-OH-TEMPO}]^+ + e^-$	0 V	*RT*	Stable capacity for 100 cycles (little crossover) NaCl as supporting electrolyte	[45]
Vanadium Acetylacetonate	$V(acac)_3 + e^- \rightarrow [V(acac)_3]^-$	$V(acac)_3 \rightarrow [V(acac)_3]^+ + e^-$	More than 1 V	*RT*	Non-aqueous, very low efficiencies, Also has some V(V) forming, but can't react with acetonitrile?	[81]
$[Ru(bpy)_3](BF4)_2$	$[Ru(bpy)_3]^{2+} + e^- \rightarrow [Ru(bpy)_3]^+$	$[Ru(bpy)_3]^{2+} \rightarrow [Ru(bpy)_3]^{3+} + e^-$	NA	*20-30*	Very low concentrations. Review stated there is no point for further research. Other metal complexes are possible as well, such as Fe or Co	[82]
$Ru(acac)_3$	$[Ru(acac)_3] + e^- \rightarrow [Ru(acac)_3]^-$	$[Ru(acac)_3] \rightarrow [Ru(acac)_3]^+ + e^-$	NA	NA	Acetonitrile solvent Non-efficient, side reactions	[83]
$Cr(acac)_3$	$[Cr(acac)_3] + e^- \rightarrow [Cr(acac)_3]^-$	$[Cr(acac)_3] \rightarrow [Cr(acac)_3]^+ + e^-$	Very large overpotential (>1 V)	*RT*	Non-aqueous (Acetonitrile), Low concentrations, low efficiencies	[84]
Li-ion hybrid RFB	$LiFePO_4$	TiO_2	Intolerably high (>0.3 V) due reaction with lithium storage materials	NA	Uses electron carrier materials to carry electrons from one side to the other	[85]

Metallocene	$Cc^+ + e^- \rightarrow Cc$	$Fc \rightarrow Fc^+ + e^-$	NA	*RT*	In Acetonitrile, Higher diffusion rates than regular V, Low concentrations	[86]
Metalbipyridyl-complexes	$Ni(II)(Bpy)_3(BF_4)_2 + 2e^- \rightarrow Ni(Bpy)_3(BF_4)_2$	$Fe(II)(Bpy)_3(BF_4)_2 \rightarrow Fe(III)(Bpy)_3(BF_4)_2 + e^-$	NA	*RT*	Non-aqueous. No useful information, only redox potential	[87]
Nonaqueous Organic Redox Flow Battery (N-methylphthalimide & 2,5-di-tert-butyl-1-methoxy-4-[2′-methoxyethoxy]benzene)	$MePh + e^- \rightarrow MePh^{\bullet -}$	DBMMB → $DBMMB^{\bullet +} + e^-$	Slight overpotential, less than 0.2 V	*RT*	Non-aqueous, many possible side reactions for $MePh^{\bullet -}$ Energy efficiency of only 69%	[88]
A symmetric organic-based non-aqueous redox flow battery PTIO: 2-phenyl-4,4,5,5-tetramethylimidazoline-1-oxyl-3-oxide	$PTIO^{\bullet} + e^- \rightarrow PTIO^-$	$PTIO^{\bullet} \rightarrow PTIO^+ + e^-$	0 V	*RT*	Non-aqueous, no crossover problems (same molecule on both sides) Stable cycling over 15 cycles. Low energy efficiency (<60 %)	[89]
All-copper Battery	$[Cu(MeCN)_4][Tf_2N]^{2+} + e^- \rightarrow [Cu(MeCN)_4][Tf_2N]^+$	$[Cu(MeCN)_4][Tf_2N] \rightarrow [Cu(MeCN)_4][Tf_2N]^+ + e^-$	NA	Minimum temperature is 66 ºC - *90 ºC*	Non-aqueous Liquid metal salt (needs 66 °C for $[Cu(MeCN)_4][Tf_2N]$ melting point)	[90]
Zinc-bromine	$Zn^{2+} + 2e^- \rightarrow Zn$	$2Br^- \rightarrow Br_2 + 2e^-$	NA	'wide range'	Uses solid Zinc	[91]
Soluble lead-acid	$Pb^{2+} + 2e^- \rightarrow Pb$	$Pb^{2+} + 2\,H_2O \rightarrow PbO_2 + 4H^+ + 2e^-$	Lead-deposition during charging results in overpotential	0-40 ºC (works at 60, loses charge efficiency due soluble PbO_2)[92]	Solid Pb and PbO_2	[92] [93] [94]
Zinc-air	$Zn(OH)_4^{2-} + 2e^- \rightarrow Zn + 4\,OH^-$	Propanol oxidation	NA	*RT*	Uses propanol as fuel to recover zinc electrolyte, metallic zinc during discharge	[95]

Li-Iodine	$Li^+ + e^- \rightarrow Li(s)$	$3I^- \rightarrow I_3^- + 2e^-$	NA	*15 – 55 ºC*	Only Cathode flow (I^-/I_3^-), Li is solid metal	[96]
Iron Chloride	$FeCl_2 + 2e^- \rightarrow Fe + 2Cl^-$	$FeCl_2 + Cl^- \rightarrow FeCl_3 + e^-$	NA	*RT* but mentioned higher operating T	Solid metallic iron on the electrode	[97]
Iron-Cadmium	$Cd^{2+} + 2e^- \rightarrow Cd$	$Fe^{2+} \rightarrow Fe^{3+} + e^-$	NA	*RT*	Metallic Cd deposition during charging, little crossover, Cadmium handling	[98]
All-neptunium	$Np^{4+} + e^- \rightarrow Np^{3+}$	$NpO_2^+ \rightarrow NpO_2^{2+} + e^-$	NA	NA	High energy efficiency, very radioactive	[99] [100]
All-uranium	$U^{4+} + e^- \rightarrow U^{3+}$	$UO_2^+ \rightarrow UO_2^{2+} + e^-$	NA	NA	Uranium(V) is unstable in water, need aprotic solvents, radioactive materials	[101]
Acid/Base flow battery with H_2	$2\,H_2O + 2e^- \rightarrow H_2 + 2OH^-$	$H_2 + 2\,H_2O \rightarrow 2H_3O^+ + 2e^-$	±0.4 V seems independent of current density	*20-50* Most likely large T interval	Not very high ΔS_R since H_2 is consumed and produced on both sides.	[102]
Acid-Base junction flow battery	Charge: $H_2O + NaCl \rightarrow HCl + NaOH$ Discharge: $HCl + NaOH \rightarrow H_2O + NaCl$		0 V	Most likely large T interval	No long cycling stability, (Energy efficiency drops significantly after 7-8 cycles)	[103]

*(*italic means, proven at that range*, Regular means limited by factors, such as solubility)

Appendix C: Exclusion procedure

The table in Appendix B has 44 flow batteries. The final 9 RFB systems were selected in 3 steps. In this Appendix more detail will be given which batteries were excluded in each step and why.

The first set of RFB systems were excluded if they fell in the following categories:

- **Solid material deposition**, a continuous flow battery cell is desired, therefore solid deposition at an electrode is not desired
- **Radioactive electrolytes**, using materials like Uranium or Neptunium is not desired, because of obvious reasons
- **Uses aqueous Mn^{3+} electrolyte**, Manganese(III) ions react with water ($2Mn^{3+} + 2H_2O \rightarrow Mn^{2+} + MnO_2 + 4\ H^+$), and form insoluble MnO_2
- **Uses aqueous Ti^{4+} electrolyte**, the performance of the Titanium couple is seriously compromised by activation polarization[46]
- **Review stated there is no point for further research [16]**, this is the case for $[Ru(bpy)_3](BF4)_2$ which has costly materials and low efficiencies. This is a strong indication the compound will not be useful for the project.

These batteries were therefore excluded from further research:

Iron-titanium; *Manganese-vanadium*; *Titanium manganese*; *$[Ru(bpy)_3](BF_4)_2$*; *Zinc-bromine*; *Soluble lead-acid*; *Zinc-air*; *Li-iodine*; *Iron chloride*; *Iron-cadmium*; *All-neptunium* and *All-uranium*

For the second cut the remaining batteries were excluded if they did not meet the following specifications:

- **Electrolytes work on a temperature interval**. The solutions need to be stable at least between 20 – 60 °C. If this cannot be reached, the electrolyte will be unusable for the application.
- **The flow battery has an overpotential smaller than 0.2 V**. If the overpotential is larger than 0.2 V, almost all energy that was converted from heat will be wasted.

The following batteries were therefore excluded from further research:

- *All-vanadium*: Uses aqueous V^{5+} electrolyte, Vanadium(V) ions react irreversibly with water above 40 °C.
- *All Copper battery*, this battery is an ionic liquid of copper, which has a melting point of 66 °C. The operating conditions are too high for our application.
- *Vanadium Polyhalide*, 80% voltaic efficiency (E^0 = 1.30 V, so overpotential is 0.26 V), also bromine gasses form at 40 °C that could hinder the performance of the hot battery[17].
- *Vanadium Bromine*, this flow battery was improved by adding HCl[17] (resulting in the polyhalide), since it is worse than the polyhalide, this one will be excluded as well.
- *Vanadium-glyoxal(O_2)*, due to oxygen polarization at the electrode, there is an overpotential.
- *Vanadium cysteine*, Too large overpotential
- *All-chromium*, the energy efficiency of this battery is extremely low (<10%) because of the overpotential due to slow kinetics at the anode
- *Vanadium Acetylacetonate*, Really large overpotential (>1V)

- *$Ru(acac)_3$*, Very low voltage efficiencies
- *$Cr(acac)_3$*, too large overpotential
- *Li-ion hybrid RFB*, The redox mediator molecules both result in a voltage loss of almost 0.3 V. Other redox mediators or changing the concentrations might reduce the voltage loss. But at this stage that is out of scope.
- *A symmetric organic-based non-aqueous redox flow battery*, very low voltage efficiencies (60-70%)
- *Acid/Base flow battery with H_2*, large overpotential (±0.4 V), seems almost independent of current density.

The final cut was made based on practical reasoning, the following batteries were excluded:

- *Vanadium-cerium*, Cerium(IV) salts have a low solubility. Cerium is also a rare earth metal, which makes large scale applications unfeasible.
- *Hydrogen Bromide RFB*, this RFB uses a liquid bromine solution. Bromine has a boiling point of 58.8 °C, which lies within the desired temperature interval. There have been reports of a bromine system which resulted into bubbles and changed α coefficients, and therefore it is decided to exclude bromine containing systems[12].
- *Metal-free organic redox molecules: 9,10-anthraquinone-2,7-disulfonic acid (AQDS)*,this system also uses bromine.
- *Bromine-Polysulfide*, This system also uses bromine.
- *Aqueous polymer based*, This system requires complex synthesis, which is out of scope for this thesis.
- *Total Organic aqueous with Methyl Viologen and 4-HO-TEMPO*, Methyl Viologen and 4-OH-TEMPO are not readily available at large quantities and require either complex synthesis or have to be bought for high prices at low quantities.
- *Metallocene*, This system uses non-aqueous solvents. In order to keep the thermodynamics simple, it was decided to stick with just aqueous systems since more data is available for these.
- *Metalbipyridyl-complexes*, Also uses non-aqueous solvents
- *Nonaqueous Organic Redox Flow Battery (N-methylphthalimide & 2,5-di-tert-butyl-1-methoxy-4-[2'-methoxyethoxy]benzene)*, Also uses non-aqueous solvents
- *Acid-Base junction flow battery*, This system requires 4 membranes and cannot be tested with our current setup. Also the energy efficiency dropped significantly after 7-8 cycles, making the system not very attractive for further applications.
- *Tiron-Pb*, Tiron has a relatively low solubility (up to 0.3 M at max). I personally preferred to avoid a Pb-based system because of the toxicity

Appendix D: ^{1}H-NMR Measurements

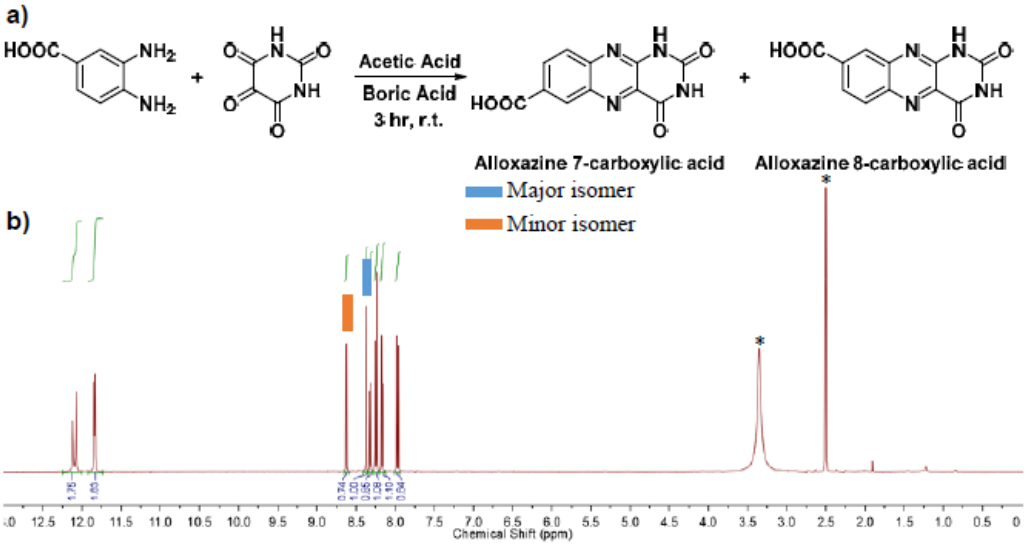

Supplementary Figure 2. (a) Synthetic scheme of alloxazine 7/8-carboxylic acid. **(b)** ^{1}H NMR (500 MHz, DMSO-d_6) spectrum of alloxazine 7/8-carboxylic acid. Major isomer: δ 12.02 (s, 1H), 11.79 (s, 1H), 8.29 (d, J = 1.9 Hz, 1H), 8.18 (d, J = 8.8 Hz, 1H), 8.09 (dd, J = 1.9, 8.8 Hz, 1H). Minor isomer: δ 12.06 (s, 1H), 11.80 (s, 1H), 8.55 (d, J = 2.0 Hz, 1H), 8.25 (dd, J = 2.0, 8.8 Hz, 1H), 7.90 (d, J = 8.8 Hz, 1H). Solvent peaks are labeled with asterisks. Final yield: 95%.

Figure D-1: ^{1}H-NMR Spectrum of ACA by Lin *et al.*[44]

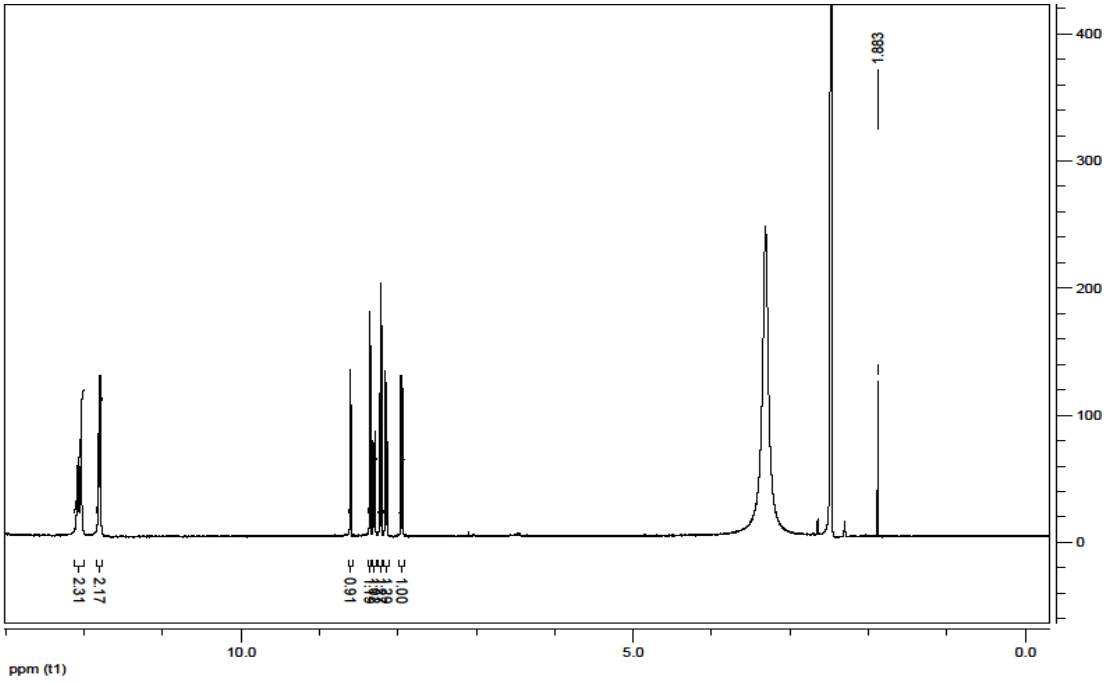

Figure D-2: ^{1}H-NMR Spectrum of ACA. This was done by dissolving 10 mg of ACA in DMSO-d^6. The NMR spectra were recorded with a 400 MHz pulsed Fourier transform NMR spectrometer.

Appendix E: Photo of the ACA-reducing setup

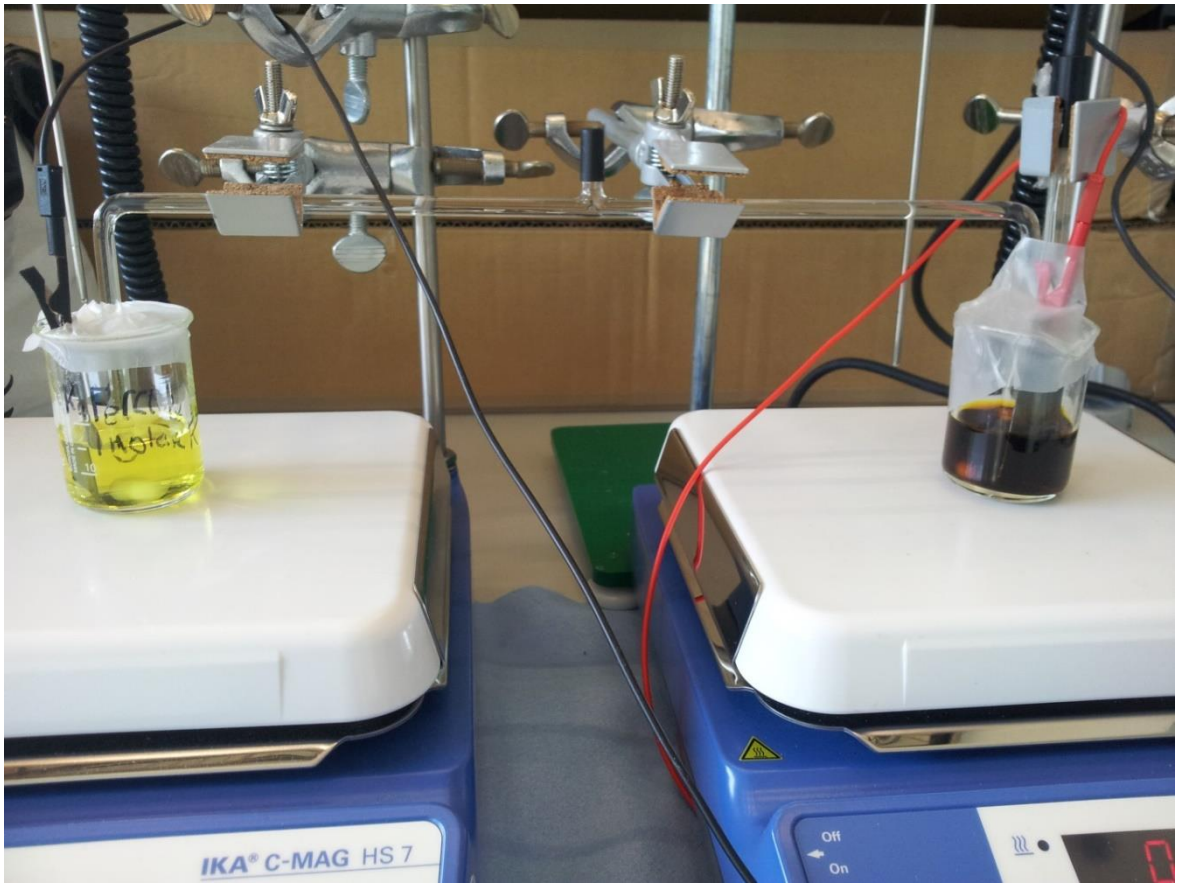

Figure E-1. Photo of the ACA reduction setup. two graphite foil electrodes of 2 cm^2 were used. A 1 M KCl salt bridge was used to connect the $K_4Fe(CN)_6$ beaker with the ACA beaker.

Appendix F: List of chemical suppliers

This section is split into the different parts of the project, for every chemical it will be shown as follows:

Chemical – purity – supplier

ACA synthesis:

- Acetic Acid, Glacial – 99.7+% – Alfa Aesar
- Alloxane monohydrate – 98% – Alfa Aesar
- Boric Acid – 99.8% – Alfa Aesar
- Diethyl ether – 99.0+% – Aldrich
- 3,4-Diaminobenzoic acid – 97% – Aldrich

Seebeck coefficient determination:

- KI – 99+% – Aldrich
- I_2 – 99.99+% – Sigma Aldrich
- KOH – 45 w/v% aq. – Alfa Aesar
- KCl – 99.5% – EMSURE
- $K_3Fe(CN)_6$ – 99.0% – Alfa Aesar
- $K_4Fe(CN)_6 \cdot 3H_2O$ – 98.5-102.0% – Alfa Aesar

Cleaning of electrodes:

- Sulfuric acid – 6.0 N – Alfa Aesar

Flow cell electrolytes:

- KI – 99% – Alfa Aesar
- I_2 – 99+% – Alfa Aesar
- $K_3Fe(CN)_6$ – 99.0% – Alfa Aesar
- $K_4Fe(CN)_6 \cdot 3H_2O$ – 98.5-102.0% – Alfa Aesar
- KCl – 99.5% – EMSURE

Appendix G: Autodesk drawings of the flow cell parts

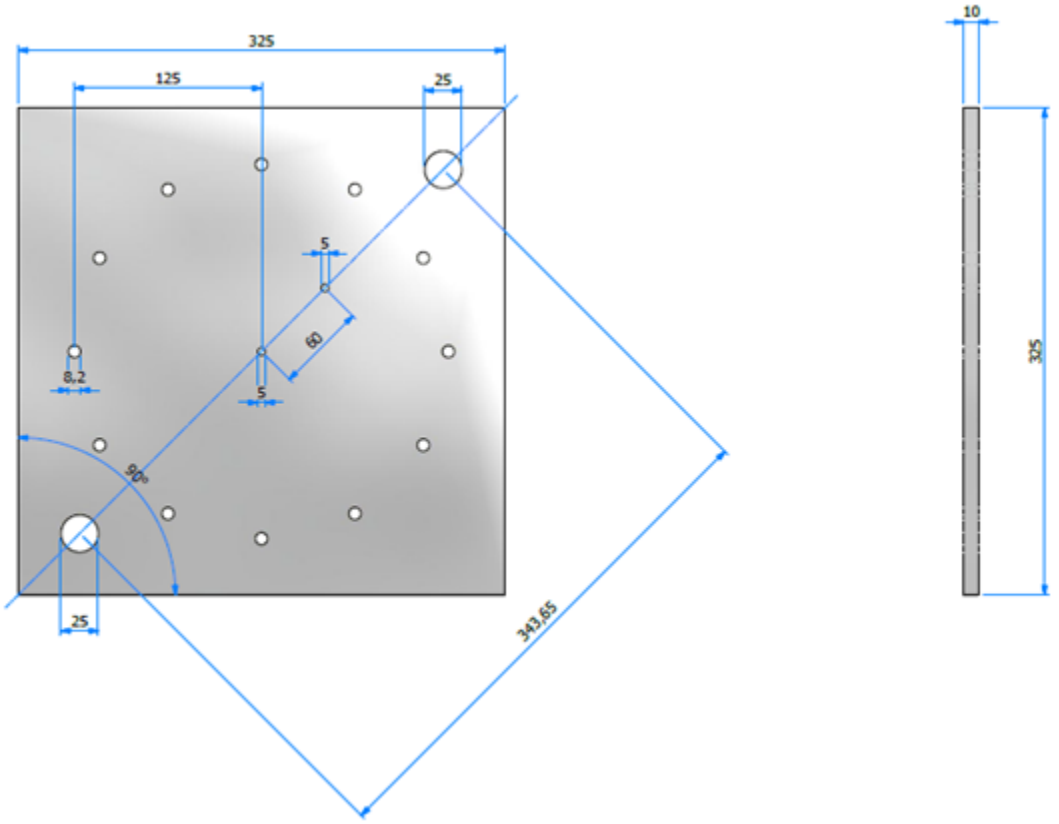

Figure G-1. Blueprint of the Aluminium support plate. All sizes are in mm.

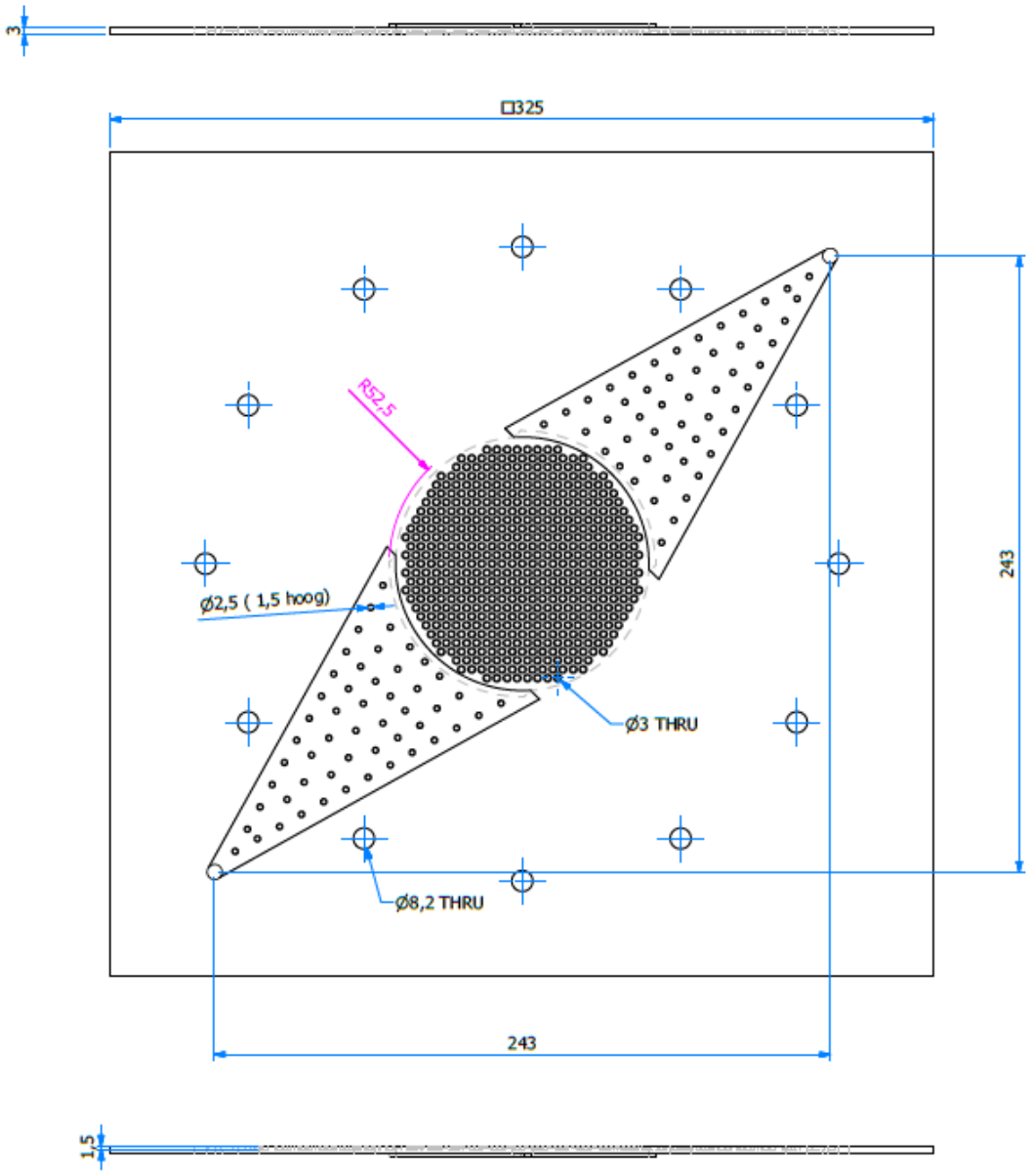

Figure G-2. Blueprint of the PA2200 Spacer. All sizes are in mm.

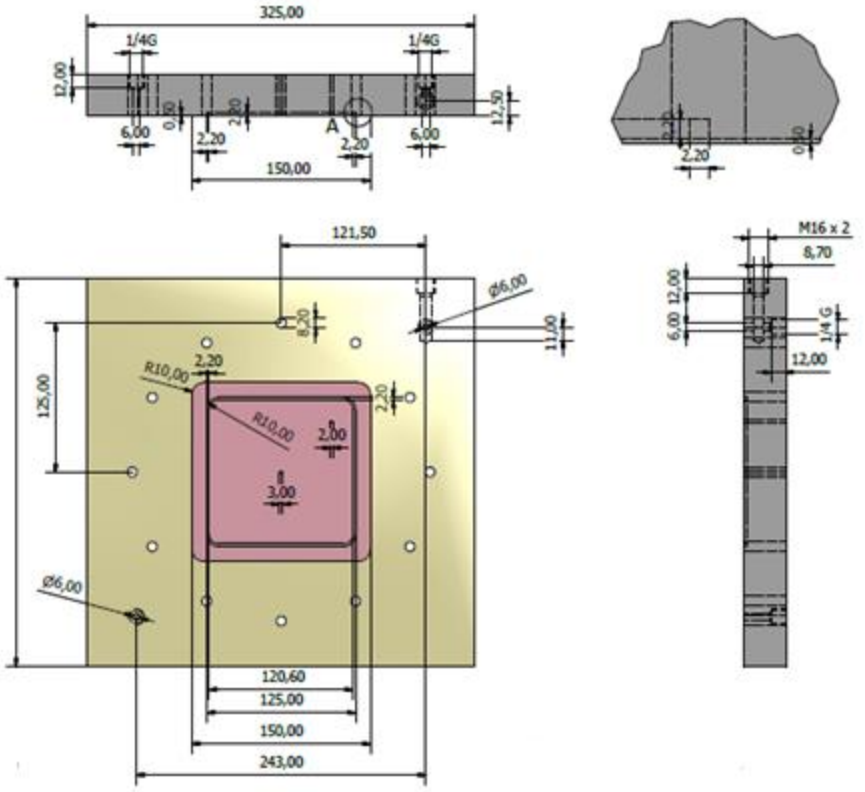

Figure G-3. Blueprint of the Teflon Back plate. All sizes are in mm. 1/4G and M16x2 indicates screw thread size.

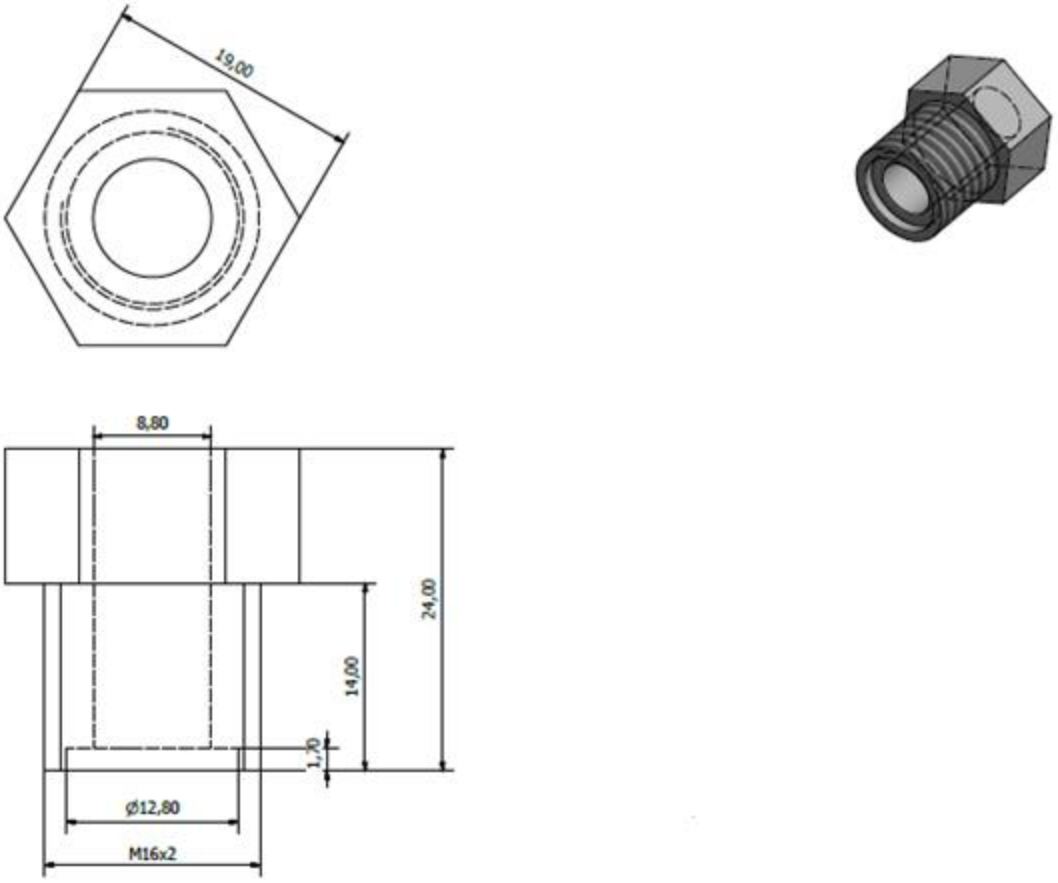

Figure G-4. Blueprint of the Teflon Reference electrode screw. All sizes are in mm.

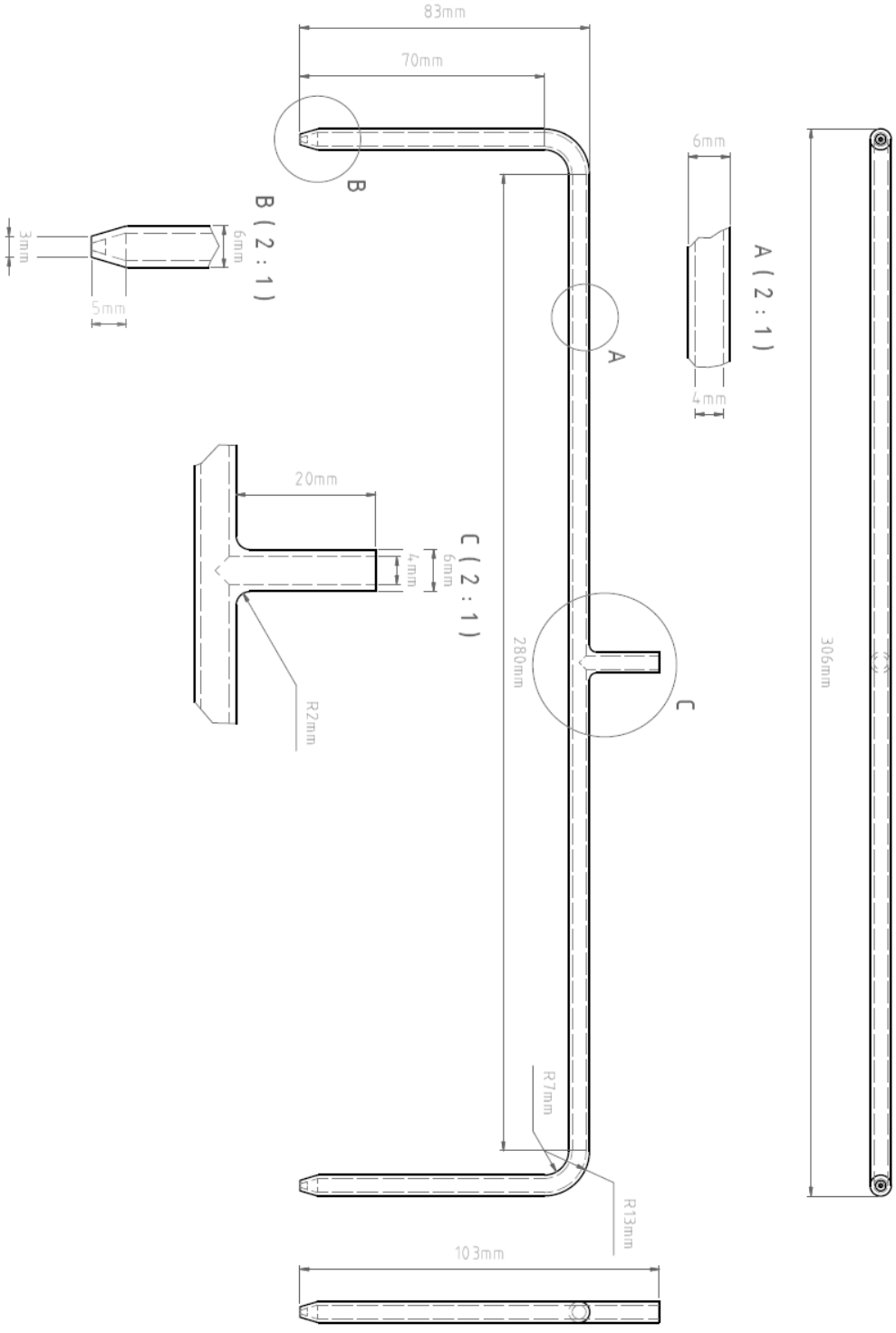

Figure G-5. Blueprint of the Salt bridge. All sizes are in mm. The salt bridge is shown from various angles.

References

[1] https://www.eia.gov/electricity/annual/html/epa_08_02.html.

[2] https://www.eia.gov/tools/faqs/faq.php?id=107&t=3.

[3] O. M. Al-Rabghi, M. Beirutty, M. Akyurt, Y. Najjar, and T. Alp, "Recovery and utilization of waste heat," *Heat Recovery Systems and CHP,* vol. 13, pp. 463-470, 1993/09/01 1993.

[4] J. Ringler, M. Seifert, V. Guyotot, and W. Hübner, "Rankine Cycle for Waste Heat Recovery of IC Engines," 2009.

[5] *U.S. Department of Energy Industrial Technologies Program report: "Waste Heat Recovery – technical and Opportunities in U.S. Industry, prepared by BCS, Inc. March 2008"*.

[6] S. Carnot, "Reflections on the motive power of fire, and on machines fitted to develop that power," *Paris: Bachelier,* 1824.

[7] M. Imran, B. S. Park, H. J. Kim, D. H. Lee, M. Usman, and M. Heo, "Thermo-economic optimization of Regenerative Organic Rankine Cycle for waste heat recovery applications," *Energy Conversion and Management,* vol. 87, pp. 107-118, 11// 2014.

[8] Rijkswaterstaat, *https://waterinfo.rws.nl/#!/kaart/watertemperatuur/,* 2017.

[9] H. Lee, *"Optimal Design of Thermoelectric Generators for Low Grade Heat Recovery",* 2014.

[10] A. W. Van Herwaarden and P. M. Sarro, "Thermal sensors based on the seebeck effect," *Sensors and Actuators,* vol. 10, pp. 321-346, 11/12/ 1986.

[11] T. I. Quickenden and Y. Mua, "A Review of Power Generation in Aqueous Thermogalvanic Cells," *Journal of The Electrochemical Society,* vol. 142, pp. 3985-3994, November 1, 1995 1995.

[12] A. Gunawan, C.-H. Lin, D. A. Buttry, V. Mujica, R. A. Taylor, R. S. Prasher*, et al.*, "Liquid Thermoelectrics: Review of Recent And Limited New Data of Thermogalvanic Cell Experiments," *Nanoscale and Microscale Thermophysical Engineering,* vol. 17, pp. 304-323, 2013/11/01 2013.

[13] S. W. Lee, Y. Yang, H.-W. Lee, H. Ghasemi, D. Kraemer, G. Chen*, et al.*, "An electrochemical system for efficiently harvesting low-grade heat energy," *Nature Communications,* vol. 5, p. 3942, 05/21/online 2014.

[14] M. Imran, M. Usman, B.-S. Park, and D.-H. Lee, "Volumetric expanders for low grade heat and waste heat recovery applications," *Renewable and Sustainable Energy Reviews,* vol. 57, pp. 1090-1109, 5// 2016.

[15] P. T. Kissinger and W. R. Heineman, "Cyclic voltammetry," *Journal of Chemical Education,* vol. 60, p. 702, 1983/09/01 1983.

[16] M. Skyllas-Kazacos, M. H. Chakrabarti, S. A. Hajimolana, F. S. Mjalli, and M. Saleem, "Progress in Flow Battery Research and Development," *Journal of The Electrochemical Society,* vol. 158, pp. R55-R79, 2011.

[17] M. Skyllas-Kazacos, G. Kazacos, G. Poon, and H. Verseema, "Recent advances with UNSW vanadium-based redox flow batteries," *International Journal of Energy Research,* vol. 34, pp. 182-189, 2010.

[18] G. Kear, A. A. Shah, and F. C. Walsh, "Development of the all-vanadium redox flow battery for energy storage: a review of technological, financial and policy aspects," *International Journal of Energy Research,* vol. 36, pp. 1105-1120, 2012.

[19] C. Ponce de León, A. Frías-Ferrer, J. González-García, D. A. Szánto, and F. C. Walsh, "Redox flow cells for energy conversion," *Journal of Power Sources,* vol. 160, pp. 716-732, 9/29/ 2006.

[20] J. R. Varcoe, P. Atanassov, D. R. Dekel, A. M. Herring, M. A. Hickner, P. A. Kohl*, et al.*, "Anion-exchange membranes in electrochemical energy systems," *Energy & Environmental Science,* vol. 7, pp. 3135-3191, 2014.

[21] E. Guler, Y. Zhang, M. Saakes, and K. Nijmeijer, "Tailor-Made Anion-Exchange Membranes for Salinity Gradient Power Generation Using Reverse Electrodialysis," *ChemSusChem,* vol. 5, pp. 2262-2270, 2012.
[22] H. Miyoshi, "Diffusion coefficients of ions through ion excange membrane in Donnan dialysis using ions of different valence," *Journal of Membrane Science,* vol. 141, pp. 101-110, 4/1/ 1998.
[23] R. H. Hammond and W. M. Risen, "An electrochemical heat engine for direct solar energy conversion," *Solar Energy,* vol. 23, pp. 443-449, 1979/01/01 1979.
[24] A. J. deBethune, T. S. Licht, and N. Swendeman, "The Temperature Coefficients of Electrode Potentials: The Isothermal and Thermal Coefficients—The Standard Ionic Entropy of Electrochemical Transport of the Hydrogen Ion," *Journal of The Electrochemical Society,* vol. 106, pp. 616-625, July 1, 1959 1959.
[25] T. I. Quickenden and C. F. Vernon, "Thermogalvanic conversion of heat to electricity," *Solar Energy,* vol. 36, pp. 63-72, 1986/01/01/ 1986.
[26] *NIST Chemistry WebBook, NIST Standard Reference Database Number 69*: National Institute of Standards and Technology, 2005.
[27] W. M. Haynes, *CRC handbook of chemistry and physics*: CRC press, 2014.
[28] T. Kim, J. S. Lee, G. Lee, H. Yoon, J. Yoon, T. J. Kang*, et al.*, "High thermopower of ferri/ferrocyanide redox couple in organic-water solutions," *Nano Energy,* vol. 31, pp. 160-167, 1// 2017.
[29] C. Caspers, "Estudos eletroquímicos de uma célula termogalvânica de cobre empregando diferentes líquidos iônicos como eletrólito," 2012.
[30] D. W. Gerlach and T. A. Newell, "Basic modelling of direct electrochemical cooling," *International journal of energy research,* vol. 31, pp. 439-454, 2007.
[31] D. W. Gerlach and T. Newell, "An investigation of electrochemical methods for refrigeration," Air Conditioning and Refrigeration Center. College of Engineering. University of Illinois at Urbana-Champaign.2004.
[32] A. Gunawan, "Electrolyte-and Transport-Enhanced Thermogalvanic Energy Conversion," Arizona State University, 2015.
[33] T. J. Kang, S. Fang, M. E. Kozlov, C. S. Haines, N. Li, Y. H. Kim*, et al.*, "Electrical power from nanotube and graphene electrochemical thermal energy harvesters," *Advanced Functional Materials,* vol. 22, pp. 477-489, 2012.
[34] K. Itaya, T. Ataka, and S. Toshima, "Spectroelectrochemistry and electrochemical preparation method of Prussian blue modified electrodes," *Journal of the American Chemical Society,* vol. 104, pp. 4767-4772, 1982.
[35] Y. Freile-Pelegrín, T. Madera-Santana, D. Robledo, L. Veleva, P. Quintana, and J. Azamar, "Degradation of agar films in a humid tropical climate: Thermal, mechanical, morphological and structural changes," *Polymer Degradation and Stability,* vol. 92, pp. 244-252, 2007.
[36] A. A. Lindén, M. Johansson, N. Hermanns, and J.-E. Bäckvall, "Efficient and Selective Sulfoxidation by Hydrogen Peroxide, Using a Recyclable Flavin−[BMIm]PF6 Catalytic System," *The Journal of Organic Chemistry,* vol. 71, pp. 3849-3853, 2006/05/01 2006.
[37] G. R. Fulmer, A. J. M. Miller, N. H. Sherden, H. E. Gottlieb, A. Nudelman, B. M. Stoltz*, et al.*, "NMR Chemical Shifts of Trace Impurities: Common Laboratory Solvents, Organics, and Gases in Deuterated Solvents Relevant to the Organometallic Chemist," *Organometallics,* vol. 29, pp. 2176-2179, 2010/05/10 2010.
[38] D. A. Vermaas and W. A. Smith, "Synergistic Electrochemical CO2 Reduction and Water Oxidation with a Bipolar Membrane," *ACS Energy Letters,* vol. 1, pp. 1143-1148, 2016/12/09 2016.
[39] DuPont, "PTFE Handbook."

[40] Masterflex, *http://www.masterflex.nl/Downloads/rz_1199.pdf*, 2017.
[41] L. Li, S. Kim, W. Wang, M. Vijayakumar, Z. Nie, B. Chen*, et al.*, "A Stable Vanadium Redox-Flow Battery with High Energy Density for Large-Scale Energy Storage," *Advanced Energy Materials,* vol. 1, pp. 394-400, 2011.
[42] S. Xiao, L. Yu, L. Wu, L. Liu, X. Qiu, and J. Xi, "Broad temperature adaptability of vanadium redox flow battery—Part 1: Electrolyte research," *Electrochimica Acta,* vol. 187, pp. 525-534, 1/1/ 2016.
[43] J. Xi, S. Xiao, L. Yu, L. Wu, L. Liu, and X. Qiu, "Broad temperature adaptability of vanadium redox flow battery—Part 2: Cell research," *Electrochimica Acta,* vol. 191, pp. 695-704, 2/10/ 2016.
[44] K. Lin, R. Gómez-Bombarelli, E. S. Beh, L. Tong, Q. Chen, A. Valle*, et al.*, "A redox-flow battery with an alloxazine-based organic electrolyte," *Nature Energy,* vol. 1, p. 16102, 07/18/online 2016.
[45] T. Liu, X. Wei, Z. Nie, V. Sprenkle, and W. Wang, "A Total Organic Aqueous Redox Flow Battery Employing a Low Cost and Sustainable Methyl Viologen Anolyte and 4-HO-TEMPO Catholyte," *Advanced Energy Materials,* vol. 6, pp. n/a-n/a, 2016.
[46] R. F. Savinell, C. C. Liu, R. T. Galasco, S. H. Chiang, and J. F. Coetzee, "Discharge Characteristics of a Soluble Iron-Titanium Battery System," *Journal of The Electrochemical Society,* vol. 126, pp. 357-360, 1979.
[47] G. Codina and A. Aldaz, "Scale-up studies of an Fe/Cr redox flow battery based on shunt current analysis," *Journal of Applied Electrochemistry,* vol. 22, pp. 668-674, 1992// 1992.
[48] Y. K. Zeng, X. L. Zhou, L. An, L. Wei, and T. S. Zhao, "A high-performance flow-field structured iron-chromium redox flow battery," *Journal of Power Sources,* vol. 324, pp. 738-744, 8/30/ 2016.
[49] W. Wang, S. Kim, B. Chen, Z. Nie, J. Zhang, G.-G. Xia*, et al.*, "A new redox flow battery using Fe/V redox couples in chloride supporting electrolyte," *Energy & Environmental Science,* vol. 4, pp. 4068-4073, 2011.
[50] W. Wang, Z. Nie, B. Chen, F. Chen, Q. Luo, X. Wei*, et al.*, "A New Fe/V Redox Flow Battery Using a Sulfuric/Chloric Mixed-Acid Supporting Electrolyte," *Advanced Energy Materials,* vol. 2, pp. 487-493, 2012.
[51] K. Gong, F. Xu, J. B. Grunewald, X. Ma, Y. Zhao, S. Gu*, et al.*, "All-Soluble All-Iron Aqueous Redox-Flow Battery," *ACS Energy Letters,* vol. 1, pp. 89-93, 2016/07/08 2016.
[52] Y. H. Wen, H. M. Zhang, P. Qian, H. T. Zhou, P. Zhao, B. L. Yi*, et al.*, "A study of the Fe(III)/Fe(II)–triethanolamine complex redox couple for redox flow battery application," *Electrochimica Acta,* vol. 51, pp. 3769-3775, 5/5/ 2006.
[53] N. Arroyo-Currás, J. W. Hall, J. E. Dick, R. A. Jones, and A. J. Bard, "An Alkaline Flow Battery Based on the Coordination Chemistry of Iron and Cobalt," *Journal of The Electrochemical Society,* vol. 162, pp. A378-A383, January 1, 2015 2015.
[54] X. Wei, G.-G. Xia, B. Kirby, E. Thomsen, B. Li, Z. Nie*, et al.*, "An Aqueous Redox Flow Battery Based on Neutral Alkali Metal Ferri/ferrocyanide and Polysulfide Electrolytes," *Journal of The Electrochemical Society,* vol. 163, pp. A5150-A5153, January 1, 2016 2016.
[55] Z. Li, G. Weng, Q. Zou, G. Cong, and Y.-C. Lu, "A high-energy and low-cost polysulfide/iodide redox flow battery," *Nano Energy,* vol. 30, pp. 283-292, 12// 2016.
[56] S. G. Bratsch, "Standard Electrode Potentials and Temperature Coefficients in Water at 298.15 K," *Journal of Physical and Chemical Reference Data,* vol. 18, pp. 1-21, 1989/01/01 1989.
[57] G. Briegleb and W. Strohmeier, "Einfluß einer Wasserstoff-Brückenbindung auf die Lichtabsorption der COOH-Gruppe," *Naturwissenschaften,* vol. 33, pp. 344-345, 1946.
[58] SigmaAldrich, *http://www.sigmaaldrich.com/catalog/product/sigma/z330418?lang=en&region=NL*, 2017.

[59] MyKinInc., "Rubber Chemical Resistance Chart," *http://mykin.com/rubber-chemical-resistance-chart-3*, 2017.
[60] M. Mäntynen, "Temperature correction coefficients of electrical conductivity and density measurements for saline groundwater," *POSIVA Oy, Eurajoki, Finland. Working report,* vol. 15, 2001.
[61] www.pressure-drop.com, "Pressure drop calculator," *http://www.druckverlust.de/Online-Rechner/dp.php*, 2017.
[62] D. A. Vermaas, M. Saakes, and K. Nijmeijer, "Doubled power density from salinity gradients at reduced intermembrane distance," *Environmental science & technology,* vol. 45, pp. 7089-7095, 2011.
[63] CrestPumpsGroup, *http://www.crestpumps.co.uk/news/use-magnetic-drive-pumps/*, 2017
[64] P. Długołęcki, A. Gambier, K. Nijmeijer, and M. Wessling, "Practical potential of reverse electrodialysis as process for sustainable energy generation," *Environmental science & technology,* vol. 43, pp. 6888-6894, 2009.
[65] C. Zhang, T. S. Zhao, Q. Xu, L. An, and G. Zhao, "Effects of operating temperature on the performance of vanadium redox flow batteries," *Applied Energy,* vol. 155, pp. 349-353, 10/1/ 2015.
[66] J. Zhang, L. Li, Z. Nie, B. Chen, M. Vijayakumar, S. Kim*, et al.*, "Effects of additives on the stability of electrolytes for all-vanadium redox flow batteries," *Journal of Applied Electrochemistry,* vol. 41, pp. 1215-1221, 2011// 2011.
[67] J. Langner, J. Melke, H. Ehrenberg, and C. Roth, "Determination of Overpotentials in All Vanadium Redox Flow Batteries," *ECS Transactions,* vol. 58, pp. 1-7, April 8, 2014 2014.
[68] M. Skyllas-Kazacos, "Novel vanadium chloride/polyhalide redox flow battery," *Journal of Power Sources,* vol. 124, pp. 299-302, 10/1/ 2003.
[69] F.-Q. Xue, Y.-L. Wang, W.-H. Wang, and X.-D. Wang, "Investigation on the electrode process of the Mn(II)/Mn(III) couple in redox flow battery," *Electrochimica Acta,* vol. 53, pp. 6636-6642, 9/20/ 2008.
[70] B. Fang, S. Iwasa, Y. Wei, T. Arai, and M. Kumagai, "A study of the Ce(III)/Ce(IV) redox couple for redox flow battery application," *Electrochimica Acta,* vol. 47, pp. 3971-3976, 9/12/ 2002.
[71] A. Paulenova, S. E. Creager, J. D. Navratil, and Y. Wei, "Redox potentials and kinetics of the Ce3+/Ce4+ redox reaction and solubility of cerium sulfates in sulfuric acid solutions," *Journal of Power Sources,* vol. 109, pp. 431-438, 7/1/ 2002.
[72] Y. Xu, Y.-H. Wen, J. Cheng, G.-P. Cao, and Y.-S. Yang, "A study of tiron in aqueous solutions for redox flow battery application," *Electrochimica Acta,* vol. 55, pp. 715-720, 1/1/ 2010.
[73] Y. H. Wen, J. Cheng, P. H. Ma, and Y. S. Yang, "Bifunctional redox flow battery-1 V(III)/V(II)–glyoxal(O2) system," *Electrochimica Acta,* vol. 53, pp. 3514-3522, 3/20/ 2008.
[74] Y. H. Wen, J. Cheng, Y. Xun, P. H. Ma, and Y. S. Yang, "Bifunctional redox flow battery: 2. V(III)/V(II)–l-cystine(O2) system," *Electrochimica Acta,* vol. 53, pp. 6018-6023, 8/20/ 2008.
[75] M. C. Tucker, K. T. Cho, F. B. Spingler, A. Z. Weber, and G. Lin, "Impact of membrane characteristics on the performance and cycling of the Br2–H2 redox flow cell," *Journal of Power Sources,* vol. 284, pp. 212-221, 6/15/ 2015.
[76] B. Huskinson, M. P. Marshak, C. Suh, S. Er, M. R. Gerhardt, C. J. Galvin*, et al.*, "A metal-free organic-inorganic aqueous flow battery," *Nature,* vol. 505, pp. 195-198, 01/09/print 2014.
[77] H. Kaku, Y.-R. Dong, K. Hanafusa, K. Moriuchi, and T. Shigematsu, "Effect of Ti(IV) Ion on Mn(III) Stability in Ti/Mn Electrolyte for Redox Flow Battery," *ECS Transactions,* vol. 72, pp. 1-9, July 27, 2016 2016.

[78] P. Zhao, H. Zhang, H. Zhou, and B. Yi, "Nickel foam and carbon felt applications for sodium polysulfide/bromine redox flow battery electrodes," *Electrochimica Acta,* vol. 51, pp. 1091-1098, 11/25/ 2005.

[79] C. Bae*, E. P. L. Roberts, M. H. Chakrabarti, and M. Saleem, "All-Chromium Redox Flow Battery for Renewable Energy Storage," *International Journal of Green Energy,* vol. 8, pp. 248-264, 2011/03/09 2011.

[80] T. Janoschka, N. Martin, U. Martin, C. Friebe, S. Morgenstern, H. Hiller*, et al.*, "An aqueous, polymer-based redox-flow battery using non-corrosive, safe, and low-cost materials," *Nature,* vol. 527, pp. 78-81, 11/05/print 2015.

[81] Q. Liu, A. E. S. Sleightholme, A. A. Shinkle, Y. Li, and L. T. Thompson, "Non-aqueous vanadium acetylacetonate electrolyte for redox flow batteries," *Electrochemistry Communications,* vol. 11, pp. 2312-2315, 12// 2009.

[82] Y. Matsuda, K. Tanaka, M. Okada, Y. Takasu, M. Morita, and T. Matsumura-Inoue, "A rechargeable redox battery utilizing ruthenium complexes with non-aqueous organic electrolyte," *Journal of Applied Electrochemistry,* vol. 18, pp. 909-914, 1988// 1988.

[83] M. H. Chakrabarti, R. A. W. Dryfe, and E. P. L. Roberts, "Evaluation of electrolytes for redox flow battery applications," *Electrochimica Acta,* vol. 52, pp. 2189-2195, 1/1/ 2007.

[84] Q. Liu, A. A. Shinkle, Y. Li, C. W. Monroe, L. T. Thompson, and A. E. S. Sleightholme, "Non-aqueous chromium acetylacetonate electrolyte for redox flow batteries," *Electrochemistry Communications,* vol. 12, pp. 1634-1637, 11// 2010.

[85] C. Jia, F. Pan, Y. G. Zhu, Q. Huang, L. Lu, and Q. Wang, "High–energy density nonaqueous all redox flow lithium battery enabled with a polymeric membrane," *Science Advances,* vol. 1, 2015.

[86] B. Hwang, M.-S. Park, and K. Kim, "Ferrocene and Cobaltocene Derivatives for Non-Aqueous Redox Flow Batteries," *ChemSusChem,* vol. 8, pp. 310-314, 2015.

[87] J. Mun, M.-J. Lee, J.-W. Park, D.-J. Oh, D.-Y. Lee, and S.-G. Doo, "Non-Aqueous Redox Flow Batteries with Nickel and Iron Tris(2,2′-bipyridine) Complex Electrolyte," *Electrochemical and Solid-State Letters,* vol. 15, pp. A80-A82, January 1, 2012 2012.

[88] X. Wei, W. Duan, J. Huang, L. Zhang, B. Li, D. Reed*, et al.*, "A High-Current, Stable Nonaqueous Organic Redox Flow Battery," *ACS Energy Letters,* vol. 1, pp. 705-711, 2016/10/14 2016.

[89] W. Duan, R. S. Vemuri, J. D. Milshtein, S. Laramie, R. D. Dmello, J. Huang*, et al.*, "A symmetric organic-based nonaqueous redox flow battery and its state of charge diagnostics by FTIR," *Journal of Materials Chemistry A,* vol. 4, pp. 5448-5456, 2016.

[90] S. Schaltin, Y. Li, N. R. Brooks, J. Sniekers, I. F. J. Vankelecom, K. Binnemans*, et al.*, "Towards an all-copper redox flow battery based on a copper-containing ionic liquid," *Chemical Communications,* vol. 52, pp. 414-417, 2016.

[91] P. Lex and B. Jonshagen, "The zinc/bromine battery system for utility and remote area applications," *Power Engineering Journal,* vol. 13, pp. 142-148, 1999.

[92] D. Pletcher and R. Wills, "A novel flow battery—A lead acid battery based on an electrolyte with soluble lead(II): III. The influence of conditions on battery performance," *Journal of Power Sources,* vol. 149, pp. 96-102, 9/26/ 2005.

[93] A. Hazza, D. Pletcher, and R. Wills, "A novel flow battery—A lead acid battery based on an electrolyte with soluble lead(II): IV. The influence of additives," *Journal of Power Sources,* vol. 149, pp. 103-111, 9/26/ 2005.

[94] J. Collins, X. Li, D. Pletcher, R. Tangirala, D. Stratton-Campbell, F. C. Walsh*, et al.*, "A novel flow battery: A lead acid battery based on an electrolyte with soluble lead(II). Part IX: Electrode and electrolyte conditioning with hydrogen peroxide," *Journal of Power Sources,* vol. 195, pp. 2975-2978, 5/1/ 2010.

[95] Y.-H. Wen, J. Cheng, S.-Q. Ning, and Y.-S. Yang, "Preliminary study on zinc–air battery using zinc regeneration electrolysis with propanol oxidation as a counter electrode reaction," *Journal of Power Sources,* vol. 188, pp. 301-307, 3/1/ 2009.

[96] Y. Zhao and H. R. Byon, "High-Performance Lithium-Iodine Flow Battery," *Advanced Energy Materials,* vol. 3, pp. 1630-1635, 2013.

[97] A. K. Manohar, K. M. Kim, E. Plichta, M. Hendrickson, S. Rawlings, and S. R. Narayanan, "A High Efficiency Iron-Chloride Redox Flow Battery for Large-Scale Energy Storage," *Journal of The Electrochemical Society,* vol. 163, pp. A5118-A5125, January 1, 2016 2016.

[98] Y. K. Zeng, T. S. Zhao, X. L. Zhou, L. Wei, and H. R. Jiang, "A low-cost iron-cadmium redox flow battery for large-scale energy storage," *Journal of Power Sources,* vol. 330, pp. 55-60, 10/31/ 2016.

[99] T. Yamamura, N. Watanabe, and Y. Shiokawa, "Energy efficiency of neptunium redox battery in comparison with vanadium battery," *Journal of Alloys and Compounds,* vol. 408–412, pp. 1260-1266, 2/9/ 2006.

[100] K. Hasegawa, A. Kimura, T. Yamamura, and Y. Shiokawa, "Estimation of energy efficiency in neptunium redox flow batteries by the standard rate constants," *Journal of Physics and Chemistry of Solids,* vol. 66, pp. 593-595, 2// 2005.

[101] T. Yamamura, K. Shirasaki, Y. Shiokawa, Y. Nakamura, and S. Y. Kim, "Characterization of tetraketone ligands for active materials of all-uranium redox flow battery," *Journal of Alloys and Compounds,* vol. 374, pp. 349-353, 7/14/ 2004.

[102] A. Sáez, V. Montiel, and A. Aldaz, "An Acid-Base Electrochemical Flow Battery as energy storage system," *International Journal of Hydrogen Energy,* vol. 41, pp. 17801-17806, 10/26/ 2016.

[103] J.-H. Kim, J.-H. Lee, S. Maurya, S.-H. Shin, J.-Y. Lee, I. S. Chang*, et al.*, "Proof-of-concept experiments of an acid-base junction flow battery by reverse bipolar electrodialysis for an energy conversion system," *Electrochemistry Communications,* vol. 72, pp. 157-161, 11// 2016.